High-Pressure NMR Investigation of Hydrogen Atom Transfer and Related Dynamic Processes in Oxo Catalysis

R. J. Klingler* and J. W. Rathke*

Contribution from the Argonne National Laboratory, Chemical Technology Division, 9700 South Cass Avenue, Argonne, Illinois 60439

*Received March 29, 1993. Revised Manuscript Received February 25, 1994**

Abstract: The cobalt center in $HCo(CO)_4$ exchanges with those in $Co_2(CO)_8$ through a facile hydride ligand transfer reaction which has been studied by ^{59}Co NMR line-shape analysis over the temperature range of 80 to 200 °C and total system pressures up to 370 atm in supercritical carbon dioxide. The lifetime of the cobalt center in $HCo(CO)_4$ varies from 2 ms at 80 °C to 10 μs at 200 °C, exhibiting an activation energy of 15.3 ± 0.4 kcal/mol. The hydride ligand transfer process is highly specific for the $HCo(CO)_4$ and $Co_2(CO)_8$ complexes. Thus, neither $Co_4(CO)_{12}$ nor $MnCo(CO)_9$ exhibit measurable chemical exchange line broadening in the ^{59}Co NMR spectra within solutions where the resonances for $HCo(CO)_4$ and $Co_2(CO)_8$ coalesce. In addition, the full peak widths at half-height ($W_{1/2}$) for the hydride, dihydrogen, and water resonances vary by less than 3 Hz in the ^1H NMR spectra, while the line widths ($W_{1/2}$) for the $HCo(CO)_4$ and $Co_2(CO)_8$ resonances broaden by more than 15 000 Hz in the ^{59}Co NMR spectra. A similar hydride ligand transfer reaction exchanges the hydride moieties in $HCo(CO)_4$ and $HMn(CO)_5$. This latter heterometallic hydride ligand transfer reaction has been investigated by ^1H NMR line-width analysis over the temperature range of 110 to 190 °C at two initial carbon monoxide concentrations, 1.39 and 4.13 M. The lifetime of the hydride moiety on the manganese center in the heterometallic hydride ligand transfer reaction between $HCo(CO)_4$ and $HMn(CO)_5$ is independent of the carbon monoxide pressure and exhibits an activation energy of 19 ± 1 kcal/mol. The ^{55}Mn NMR spectra indicate no measurable exchange (less than 30 transfers per second) between the manganese centers in $HMn(CO)_5$, $MnCo(CO)_9$, and $Mn_2(CO)_{10}$ under the same reaction conditions, where the hydride moieties in $HMn(CO)_5$ and $HCo(CO)_4$ are undergoing facile exchange (greater than 10^4 transfers per second) as evident in the ^1H NMR spectra. This lack of measurable exchange between the manganese centers in $HMn(CO)_5$, $MnCo(CO)_9$, and $Mn_2(CO)_{10}$ is inconsistent with an oxidative addition reaction mechanism for the heterometallic hydride ligand transfer reaction. Alternatively, the kinetics of these hydride ligand transfer reactions are interpreted in terms of a hydrogen atom transfer reaction mechanism involving $\cdot Co(CO)_4$ and $\cdot Mn(CO)_5$ radicals. Thus, the degenerate hydrogen atom transfer reaction between $HCo(CO)_4$ and $\cdot Co(CO)_4$ proceeds with activation parameters of $\Delta H^\ddagger = 5.5 \pm 0.6$ kcal/mol and $\Delta S^\ddagger = -16 \pm 1$ cal/(K·mol), while the endothermic hydrogen atom transfer from manganese in $HMn(CO)_5$ to cobalt in $\cdot Co(CO)_4$ exhibits an activation enthalpy of 10 ± 1 kcal/mol. In addition, the kinetics for the ligand exchange reaction between the coordinated carbonyl groups in $Co_2(CO)_8$ and free carbon monoxide has been studied in mesitylene solvent by ^{13}C NMR line-shape analysis over the temperature range of 100 to 180 °C under 8.2 M of carbon monoxide. In this temperature range, the free carbon monoxide ligand exhibits a strongly temperature-dependent chemical shift in the presence of $Co_2(CO)_8$. This temperature-dependent ^{13}CO chemical shift is interpreted as a contact chemical shift due to facile ligand exchange with $\cdot Co(CO)_4$ radicals. The resultant analysis of the contact chemical shift data yields a calculated Co–Co bond dissociation enthalpy (BDE) of 19 ± 2 kcal/mol. The magnetic susceptibility of a solution of $Co_2(CO)_8$ in carbon monoxide has been studied by ^1H NMR spectroscopy over the temperature range of 120 to 225 °C, consistently yielding an enthalpy and entropy for Co–Co bond homolysis of $\Delta H^\circ = 19 \pm 2$ kcal/mol and $\Delta S^\circ = 29 \pm 4$ cal/(K·mol). This Co–Co BDE when used in combination with the enthalpy of hydrogenation for $Co_2(CO)_8$ yields a Co–H BDE in $HCo(CO)_4$ of 59 ± 1 kcal/mol. Consistently, the activation enthalpy for hydrogen atom transfer in the $HCo(CO)_4/\cdot Co(CO)_4$ system is between 5 and 10% of the measured Co–H bond enthalpy ($\Delta H^\ddagger$/BDE = 0.093) in agreement with the theory for atom transfer reactions developed by Marcus.

Introduction

The $Co_2(CO)_8$-catalyzed hydroformylation of olefins is one of the most extensively investigated reactions in the field of organometallic chemistry.[1] Yet, relatively few spectroscopic studies have been conducted under the high-temperature and -pressure conditions that are actually employed for the industrial process.[2] Recently, we have described a high-sensitivity toroid NMR detector coil and associated pressure vessel[3] that allow the *in situ* observation of reaction intermediates under forcing reaction conditions of pressures to 300 atm and temperatures to 250 °C. Two new aspects of the hydroformylation system were immediately apparent using this spectroscopic technique to investigate the hydroformylation of propylene in supercritical carbon dioxide.[4] First, the ^{59}Co NMR spectra demonstrate the existence of an unusually facile hydride ligand exchange reaction, which equilibrates the cobalt center in $HCo(CO)_4$ with those in $Co_2(CO)_8$. Second, the olefin reduces the steady-state $HCo(CO)_4$ concentration well below its equilibrium value[2,4] based on the hydrogenation of $Co_2(CO)_8$. Yet, the olefin dependence of the resultant steady-state $HCo(CO)_4$ levels is difficult to explain[5] on the basis of the conventional Heck–Breslow[6] hydroformylation reaction mechanism[1] and warrants additional investigation. In a

* Abstract published in *Advance ACS Abstracts*, May 1, 1994.

(1) (a) Pino, P.; Piacenti, F.; Bianchi, M. In *Organic Synthesis via Metal Carbonyls*; Wender, I., Pino, P., Eds.; Wiley: New York, 1977; Vol. 2, Chapter 2. (b) Paulik, F. E. *Catal. Rev.* **1972**, *6*, 49–84. (c) Orchin, M.; Rupilius, W. *Catal. Rev.* **1972**, *6*, 85–131. (d) Pruett, R. L. *Advances in Organometallic Chemistry*; Stone, F. G. A., West, R., Eds.; Academic Press: New York, 1979; Vol. 17, pp 1–60.

(2) Mirbach, M. F. *J. Organomet. Chem.* **1984**, *265*, 205–213.

(3) (a) Rathke, J. W. *J. Magn. Reson.* **1989**, *85*, 150–155. (b) Klingler, R. J.; Rathke, J. W. *Prog. Inorg. Chem.* **1991**, *39*, 131–180.

(4) Rathke, J. W.; Klingler, R. J.; Krause, T. R. *Organometallics* **1991**, *10*, 1350–1355.

(5) Unpublished results.

0002-7863/94/1516-4772$04.50/0

related theme, Pino has reported[7] isotope distributions within the aldehyde product by employing a mixture of preformed $HCo(CO)_4$ together with D_2 in the gas phase. He found that these isotope distributions were perplexing to interpret by the Heck–Breslow mechanism. Thus, on the basis of this isotope labeling work, Pino argued for an "unknown active cobalt complex" that is more reactive than $HCo(CO)_4$ in the activation of the olefin. Taken together these observations suggest that alternative reaction pathways exist for the $HCo(CO)_4$ complex in addition to those contained in the conventional hydroformylation reaction mechanism.[1] It is further possible that these alternative reaction pathways involve an important intermediate, $^{\bullet}Co(CO)_4$ radical, that is not considered in the Heck–Breslow mechanistic scheme.

In this study we have focused in detail on the hydride ligand exchange reaction and its associated chemistry, all of which occur in the range for the temperature and carbon monoxide pressure that are typically used for the industrial hydroformylation process. The speed of the hydride ligand exchange reaction is remarkable. Thus, the equilibration of the cobalt centers between $HCo(CO)_4$ and $Co_2(CO)_8$ occurs roughly 7 orders of magnitude faster than the net rate of *n*-butyraldehyde production[4] in the hydroformylation of propylene at 80 °C. The hydride ligand exchange reaction involving $HCo(CO)_4$ and $Co_2(CO)_8$ is the type of rapid chemical equilibrium process that is ideally suited for NMR line-shape analysis. Indeed, this reaction would be difficult to investigate by almost any other experimental technique. In particular, the main goal of this NMR investigation was to determine the relative importance of the potential $Co_2(CO)_7$ and $^{\bullet}Co(CO)_4$ intermediates, at least with respect to the facile hydride ligand exchange reaction that equilibrates the cobalt centers in $HCo(CO)_4$ and $Co_2(CO)_8$. Notably, there exists sufficient precedent to dictate a careful consideration of both possible intermediates for the hydride ligand exchange reaction. Thus, a recent report[8a] has proposed that hydride ligand exchange can proceed at low carbon monoxide pressure by the oxidative addition of a series of metal hydrides to the coordinatively unsaturated cobalt center in $Co_2(CO)_7$. Alternatively, hydrogen and halogen atom transfers are well-documented to proceed through photochemically generated metal-centered radicals.[9] Fortunately, it is possible to distinguish by NMR line-shape analysis techniques between the potential oxidative addition and hydrogen atom transfer mechanisms for the hydride ligand exchange reaction that occurs in the oxo catalyst system.

The complete analysis of the hydride ligand exchange reaction required the concurrent investigation of two additional chemical equilibrium processes that are also occurring under the hydroformylation reaction conditions. The first of these additional processes is the reversible Co–Co bond homolysis in $Co_2(CO)_8$ to yield $^{\bullet}Co(CO)_4$ radicals in eq 1. The second is carbonyl

$$Co_2(CO)_8 \rightleftharpoons 2^{\bullet}Co(CO)_4 \qquad (1)$$

exchange, presumably through the coordinatively unsaturated $Co_2(CO)_7$ intermediate of eq 2. Therefore, a further goal of this

$$Co_2(CO)_8 \rightleftharpoons Co_2(CO)_7 + CO \qquad (2)$$

NMR investigation was to better define the relative energetics for the Co–Co bond homolysis process and carbonyl exchange. The activation energy for carbonyl exchange in the $Co_2(CO)_8$ system has been investigated by several workers, beginning with the ^{14}CO isotope tracer studies of Basolo and Wojcicki in the early sixties.[10] However, this carbonyl exchange reaction has not been previously investigated in the temperature range that is used industrially for the hydroformylation process. In the present work, the carbonyl exchange reaction between free and coordinated carbon monoxide in $Co_2(CO)_8$ was investigated by NMR line-shape analysis in the temperature range 100–180 °C. The resultant activation enthalpy agrees with previous determinations. Significantly, at the higher temperatures used in this study, we found that the carbon monoxide exhibits a large temperature-dependent chemical shift in the ^{13}C NMR spectra, proposedly through its interaction with the metal-centered radicals from eq 1 as indicated in eq 3. The resultant contact chemical

$$^{\bullet}Co(^{*}CO)_4 + CO \rightleftharpoons {}^{\bullet}Co(^{*}CO)_3(CO) + {}^{*}CO \qquad (3)$$

shift is not observable below 80 °C, which is the highest temperature studied in a previous NMR investigation[11] of the $Co_2(CO)_8$ system. In addition, we have determined the Co–Co bond dissociation enthalpy (BDE) for $Co_2(CO)_8$ by a variety of NMR techniques, including measurement of the magnetic susceptibility by NMR spectroscopy using a modification of Evan's method.[12]

Results

The hydrogenations of dicobalt octacarbonyl,[13,14] eq 4, and dimanganese decacarbonyl,[15] eq 5, proceed cleanly in supercritical

$$Co_2(CO)_8 + H_2 \rightleftharpoons 2HCo(CO)_4 \qquad (4)$$

$$Mn_2(CO)_{10} + H_2 \rightleftharpoons 2HMn(CO)_5 \qquad (5)$$

carbon dioxide in the temperature range 40–200 °C for the former and 160–220 °C for the latter. No unusual solvent effects were noted[16] for the supercritical fluid medium in comparison to nonpolar organic solvents. These previous studies were based on the integrated intensities of the NMR resonances for the reactions in eqs 4 and 5. However, additional information is obtainable from the NMR experiment on the basis of the NMR line shapes.[17] This investigation uses a combination of ^1H, ^{13}C, ^{59}Co, and ^{55}Mn line-width analysis techniques to probe the facile hydride ligand transfer reactions that occur in the oxo catalyst system.

Line Widths in the ^{59}Co Spectra. The full peak width at half-height ($W_{1/2}$) data of Figure 1 illustrate the temperature dependence of the ^{59}Co NMR line width for $Co_2(CO)_8$ in the presence and absence of dihydrogen. An important feature of the data in Figure 1 is the substantial temperature region, 15–150 °C, over which the line width for the ^{59}Co resonance is relatively invariant. This remarkably flat line-width dependence for a quadrupolar nucleus, ^{59}Co, is due to viscosity effects, which, in turn, influence the molecular correlation time for the NMR

(6) (a) Heck, R. F.; Breslow, D. S. *Chem. Ind.* [*London*] **1960**, 467. (b) Heck, R. F.; Breslow, D. S. *J. Am. Chem. Soc.* **1961**, *83*, 4024.
(7) Pino, P. *Ann. N.Y. Acad. Sci.* **1983**, *415*, 111–128.
(8) (a) Kovács, I.; Sisak, A.; Ungváry, F.; Markó, L. *Organometallics* **1989**, *8*, 1873–1877. (b) Nappa, M. J.; Santi, R.; Diefenbach, S. P.; Halpern, J. *J. Am. Chem. Soc.* **1982**, *104*, 619–621.
(9) (a) Eisenberg, D. C.; Norton, J. R. *Isr. J. Chem.* **1991**, *31*, 55–66. (b) Brown, T. L. Atom Transfer Reactions and Radical Chain Processes Involving Atom Transfer. In *Organometallic Radical Processes*; Trogler, W., Ed.; Elsevier: Lucerne, Switzerland, 1990. (c) Baird, M. C. *Chem. Rev.* **1988**, *88*, 1217–1227. (d) Meyer, T. J.; Caspar, J. V. *Chem. Rev.* **1985**, *85*, 187–218.
(10) Basolo, F.; Wojcicki, A. *J. Am. Chem. Soc.* **1961**, *83*, 520–528. (b) Breitschaft, S.; Basolo, F. *J. Am. Chem. Soc.* **1966**, *88*, 2702–2706.
(11) Roe, D. C. *Organometallics* **1987**, *6*, 942–946.
(12) (a) Evans, D. F. *J. Chem. Soc.* **1959**, 2003–2005. (b) Sur, S. K. *J. Magn. Reson.* **1989**, *82*, 169–173. (c) Crawford, T. H.; Swanson, J. *J. Chem. Educ.* **1971**, *48*, 382–386.
(13) Rathke, J. W.; Klingler, R. J.; Krause, T. R. *Organometallics* **1992**, *11*, 585–588.
(14) (a) Ungváry, F. *J. Organomet. Chem.* **1972**, *36*, 363–370. (b) Alemdaroglu, N. H.; Penninger, J. M. L.; Oltay, E. *Monatsh. Chem.* **1976**, *107*, 1043–1053. (c) Tannenbaum, R. Ph.D. Dissertation, Dissertation ETH No. 6970, Swiss Federal Institute of Technology, Zurich, Switzerland. (d) Iwanaga, R. *Bull. Chem. Soc. Jpn.* **1962**, *35*, 774–778.
(15) Klingler, R. J.; Rathke, J. W. *Inorg. Chem.* **1992**, *31*, 804–808.
(16) The enthalpy and entropy of hydrogenation for the cobalt system of eq 4 conducted in supercritical carbon dioxide[13] compare quite favorably with the values reported by Ungváry in *n*-heptane solvent.[14] Similarly, the observed net rate of aldehyde production in addition to the steady-state $HCo(CO)_4$ and $RC(O)Co(CO)_4$ concentrations for the hydroformylation of propylene in supercritical carbon dioxide[4] were comparable to the values reported by Mirbach for methylcyclohexane[2] solvent.

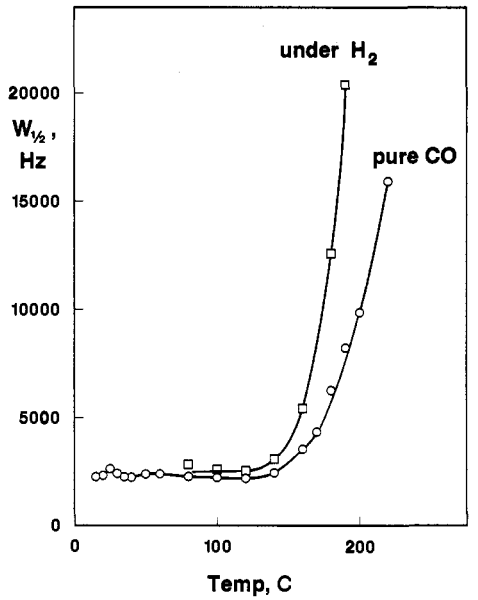

Figure 1. ^{59}Co NMR line widths: ○, 4.8 mM $Co_2(CO)_8$ in 7.1 M CO; □, 48 mM $Co_2(CO)_8$ under 2.7 M CO and 1.4 M H_2 in supercritical carbon dioxide (d = 0.5 g/mL).

substrate.[17a] Thus, there are now several examples demonstrating that NMR resonances are typically sharper by an order of magnitude in supercritical fluids relative to organic solvents due to the lower viscosities of supercritical fluid media.[3b,18] In addition, the viscosity of a gas increases only as the square root of the temperature instead of the usual exponential decrease observed for liquid solvents.[19] Therefore, a supercritical fluid medium provides for sharper NMR resonances and for a smaller temperature dependence in the resulting natural NMR line width. This feature of supercritical media is of particulate note for systems with quadrupolar nuclei.

For temperatures above 150 °C, the ^{59}Co NMR line width in Figure 1 increases more rapidly than the $T^{1/2}$ baseline dependence of the natural line width. This rapid change in the transverse spin relaxation time for the ^{59}Co nucleus is due to the onset of chemical reaction processes that affect the $Co_2(CO)_8$ molecule. Qualitatively, the ^{59}Co line width ($W_{1/2}$) is inversely proportional to the lifetime of a cobalt center in the $Co_2(CO)_8$ molecule.[17] Furthermore, the close similarity of the curves in Figure 1 suggests that a common chemical process exists both in the presence and absence of dihydrogen, although the lifetime of the cobalt center in $Co_2(CO)_8$ appears to be somewhat shorter when dihydrogen is added to the system. The more detailed mechanistic analysis of the following sections underscores these qualitative observations.

Cobalt Center Exchange between $HCo(CO)_4$ and $Co(CO)_8$. The stacked plot in Figure 2 illustrates the gradual broadening and collapse of the ^{59}Co resonance for $Co_2(CO)_8$, −2200 ppm, with that for $HCo(CO)_4$, −3055 ppm, as the temperature approaches 200 °C. The spectral changes in Figure 2 are completely reversible with temperature. Furthermore, not all ^{59}Co resonances broaden in this manner. Thus, equilibrium concentrations of $Co_4(CO)_{12}$ are produced from $Co_2(CO)_8$ by carefully controlling the temperature and CO pressure, resulting in the spectrum of Figure 3. This spectrum demonstrates that the $Co_4(CO)_{12}$ resonance remains distinct at a temperature where

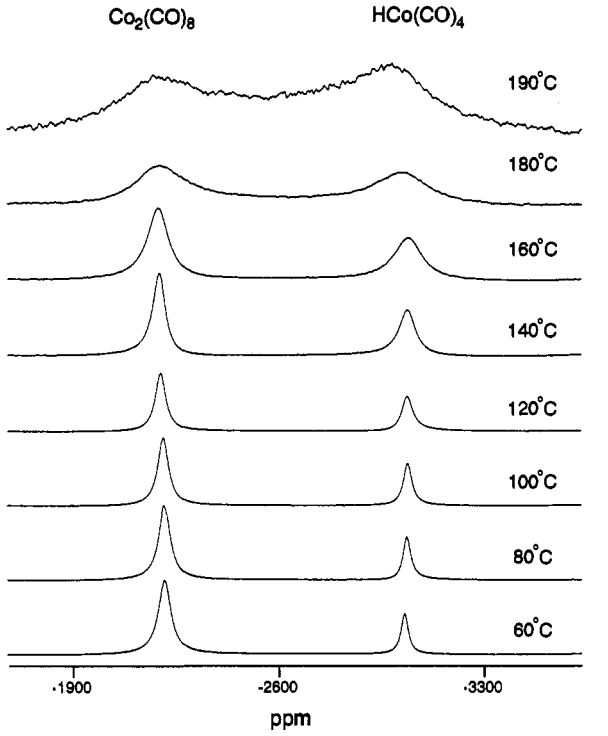

Figure 2. ^{59}Co NMR spectra for the reaction of 48 mM $Co_2(CO)_8$ under 2.7 M CO and 1.4 M H_2 in supercritical carbon dioxide (d = 0.5 g/mL).

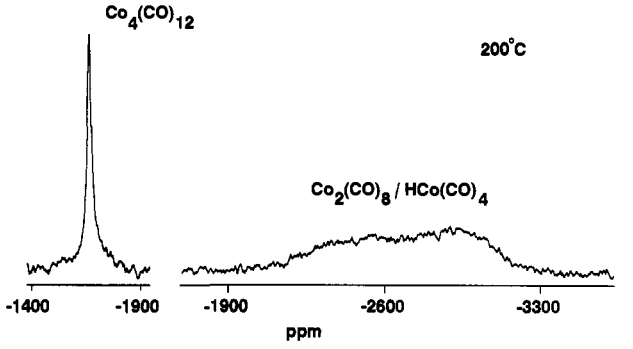

Figure 3. ^{59}Co NMR spectrum at 200 °C containing 0.021 M $Co_4(CO)_{12}$ under 5.5 M CO and 1.4 M H_2 in supercritical carbon dioxide (d = 0.5 g/mL).

the $HCo(CO)_4$ and $Co_2(CO)_8$ resonances have already collapsed to a broad multiplet. Similarly, the proton signals remain sharp throughout the entire 34–200 °C temperature range, as demonstrated at 180 °C in Figure 4.

Several features with respect to Figure 4 deserve comment. First, the ^{1}H NMR line widths change by less than 3 Hz, while the ^{59}Co line widths increase by more than 15 000 Hz in Figures 1 and 2. Therefore, the line broadening evident in the ^{59}Co NMR spectra of Figure 2 is not due to a general nuclear spin-electron spin magnetic dipole–dipole relaxation process, which could result from the buildup of macroscopic concentrations of a paramagnetic species.[17] Instead, the line broadening evident in Figure 2 is a specific process which only affects the transverse spin relaxation times of the cobalt centers in $HCo(CO)_4$ and $Co_2(CO)_8$. The sharpness of the $Co_4(CO)_{12}$ spectrum in Figure 3 also demonstrates the selectivity of the exchange process for the cobalt centers in $HCo(CO)_4$ and $Co_2(CO)_8$. Second, the chemical shift environment of the hydride moiety does not change significantly in the process which equilibrates the cobalt centers in Figure 2, because the hydride resonance remains sharp in the ^{1}H NMR spectrum. Third, the line widths of the resonances for dihydrogen, 4.5 ppm, and water, 0.8 ppm, also vary by less than 3 Hz in the ^{1}H NMR

(17) (a) Carrington, A.; McLachlan, A. D. *Introduction to Magnetic Resonance*; Harper & Row: New York, 1967; Chapters 11–13. (b) Ernst, R. R.; Bodenhauser, G.; Wokaun, A. *Principles of Nuclear Magnetic Resonance in One and Two Dimensions*; Clarendon Press: Oxford, 1987; Chapter 2. (c) Redfield, A. G. *Adv. Magn. Reson.* **1965**, *1*, 1–32.

(18) (a) Robert, J. M.; Evilia, R. F. *J. Am. Chem. Soc.* **1985**, *107*, 3733–3735. (b) Lamb, D. M.; Vander Velde, D. G.; Jonas, J. *J. Magn. Reson.* **1987**, *73*, 345–348.

(19) Moore, W. J. *Physical Chemistry*, 3rd ed.; Prentice-Hall Inc.: Englewood Cliffs, NJ, 1962; Chapter 7.

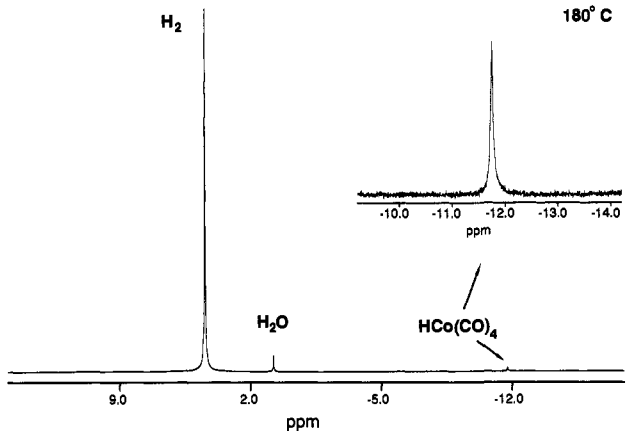

Figure 4. ^{1}H NMR spectrum at 180 °C. Conditions are as in Figure 2.

spectra, indicating that these species are not involved in the process which equilibrates the cobalt centers in Figure 2.

These observations indicate that the coalescence of the ^{59}Co NMR resonances in Figure 2 is best described by a simple two-site exchange process involving only the cobalt complexes as indicated in eq 6. The NMR line-shape analysis for the two-site

$$H^*Co(CO)_4 + Co_2(CO)_8 \rightleftharpoons HCo(CO)_4 + Co^*Co(CO)_8 \quad (6)$$

exchange system of Figure 2 and eq 6 is simplified by the lack of coupling between the exchanging cobalt centers. Furthermore, hyperfine coupling to the hydride or carbonyl groups is expected but is not resolvable with a natural ^{59}Co NMR line width of nearly 2200 Hz, as indicated in Figure 1. In addition, there is no experimental evidence to invoke $Co_4(CO)_{12}$ as a third exchanging cobalt site either as a reaction intermediate or as a byproduct of the exchange process in eq 6. Thus, $Co_4(CO)_{12}$ was not observable under the conditions of Figure 2, and even at highly elevated temperatures, where the equilibrium $Co_4(CO)_{12}$ concentration is detectable, there was no indication that $Co_4(CO)_{12}$ enters into the cobalt center exchange on the time scale of the process in eq 6, as demonstrated in Figure 3. In addition, the trace quantities of an unidentified cobalt species[4] with a ^{59}Co NMR resonance at −1370 ppm remains sharp and does not exchange at a measurable rate with the cobalt centers in $HCo(CO)_4$ or $Co_2(CO)_8$ under these reaction conditions. The experimental spectra were fit by a standard least-squares approach to a two-site exchange process, as described in greater detail in the Experimental Section. The calculated spectra are plotted with smooth curves through the experimental data points in Figure 5. The resultant line-shape analysis provides a measure of the lifetimes for the cobalt centers in each of the two chemical environments defined in eq 6. However, the $HCo(CO)_4$ and $Co_2(CO)_8$ lifetimes are not completely independent parameters. The ratio of these lifetimes at any given temperature is directly proportional to the ratio of the bulk $HCo(CO)_4$ and $Co_2(CO)_8$ concentrations, which are controlled by the thermodynamics[13,14] for the hydrogenation in eq 4. Accordingly, the lifetime of the cobalt center in $HCo(CO)_4$ will be used as a single measure of the facility for the exchange in eq 6, yielding an activation energy of 15.3 ± 0.4 kcal/mol in the Arrhenius plot of the right side of Figure 5.

Hydride Ligand Exchange between $HCo(CO)_4$ and $HMn(CO)_5$. The mixed-metal system obtained by adding $Mn_2(CO)_{10}$ to the cobalt system of Figure 2 helps to clarify the underlying chemistry of the exchange process in eq 6. At temperatures below 100 °C the hydride resonances for $HMn(CO)_5$ and $HCo(CO)_4$ are distinguishable in the ^{1}H NMR spectra at −7.8 and −11.7 ppm in Figure 6. The two hydride resonances gradually merge to a single line at approximately 160 °C. This observation demonstrates that at 160 °C the two hydride centers are interconverting at a rate that is comparable to the difference in their chemical shifts,[20] or approximately 10^3 hydride transfers per second in eq 7. Thus, the time scale of the heterometallic hydride ligand

$$^*HMn(CO)_5 + HCo(CO)_4 \rightleftharpoons HMn(CO)_5 + {}^*HCo(CO)_4 \quad (7)$$

exchange in eq 7 is roughly 1 order of magnitude slower than the cobalt center exchange of eq 6, but it is still many orders of magnitude faster than most of the conventional catalytic processes which occur with these metal complexes: the hydrogenation in eqs 4 and 5, the water-gas shift reaction, or the hydroformylation of propylene. The ^{1}H NMR spectra in Figure 6 were fit by a standard least-squares approach to the two-site exchange equilibrium of eq 7, and the calculated curves are plotted through the experimental data points. This line-width analysis for the hydride ligands is not complicated by scalar coupling to the quadrupolar metal nuclei, as explained in the Experimental Section. The resultant first-order lifetime of the hydride moiety on the manganese center is independent of the carbon monoxide pressure to within the scatter of the data as shown in Figure 6 for two initial carbon monoxide pressures, which differ by a factor of 3.

Consistent with the cobalt system of eq 6, the line widths of the corresponding resonances for dihydrogen and water change by less than 3 Hz from 80 to 190 °C, while the hydride resonances for $HMn(CO)_5$ and $HCo(CO)_4$ are coalescing in Figure 6 due to the process in eq 7. Qualitatively, the presence of $HMn(CO)_5$ has no significant effect on the ^{59}Co line widths when compared to Figure 2. This is consistent with the observation that heterometallic hydride ligand exchange in eq 7 is 1 order of magnitude slower than the exchange which is already occurring between the cobalt centers alone in eq 6. The ^{59}Co NMR line widths were not quantitatively analyzed in the mixed-metal system, in part because they are further complicated by the presence of a third cobalt-containing species,[15] $MnCo(CO)_9$. However, the $MnCo(CO)_9$ dimer does not appear to enter into the cobalt center exchange on the time scale of the process in eq 6. At 200 °C the $MnCo(CO)_9$ resonance is clearly visible in the ^{59}Co NMR spectrum as a distinct sharp peak on top of the broad multiplet formed by the coalescence of the $HCo(CO)_4$ and $Co_2(CO)_8$ resonances, similar to the result for $Co_4(CO)_{12}$ in Figure 3.

In marked contrast to the rapid temperature variation exhibited by the ^{59}Co spectra in Figures 1 and 2, the corresponding ^{55}Mn NMR spectra show minimal temperature dependence. Thus, the ^{55}Mn line width ($W_{1/2}$) for $HMn(CO)_5$ varies by less than 50 Hz over the temperature range of 100 to 200 °C as indicated in Tables 5 and 6 of the supplementary material. In contrast, a chemical reaction which leads to the exchange of the manganese centers in $HMn(CO)_5$, $MnCo(CO)_9$, and $Mn_2(CO)_{10}$ would result in additional broadening of these ^{55}Mn NMR resonances according[20] to eq 8, where τ is the lifetime of the NMR substrate

$$W_{1/2}(\text{obs}) = W_{1/2}^* + 1/\pi\tau \quad (8)$$

and $W_{1/2}^*$ is the line width in the absence of chemical exchange. The lack of significant $W_{1/2}$ variation for the ^{55}Mn NMR line widths in Tables 5 and 6 indicates that the manganese center exchange of eq 9, which is analogous to the cobalt center exchange

$$H^*Mn(CO)_5 + Mn_2(CO)_{10} \rightleftharpoons HMn(CO)_5 + Mn^*Mn(CO)_{10} \quad (9)$$

of eq 6, is too slow to observe by measurements of the ^{55}Mn

(20) (a) Johnson, C. S. *Adv. Magn. Reson.* **1965**, *1*, 33–101. (b) Eaton, D. R. In *Physical Methods in Advanced Inorganic Chemistry*; Hill, H. A., Day, P., Eds.; Wiley-Interscience: New York, 1968; pp 462–537.

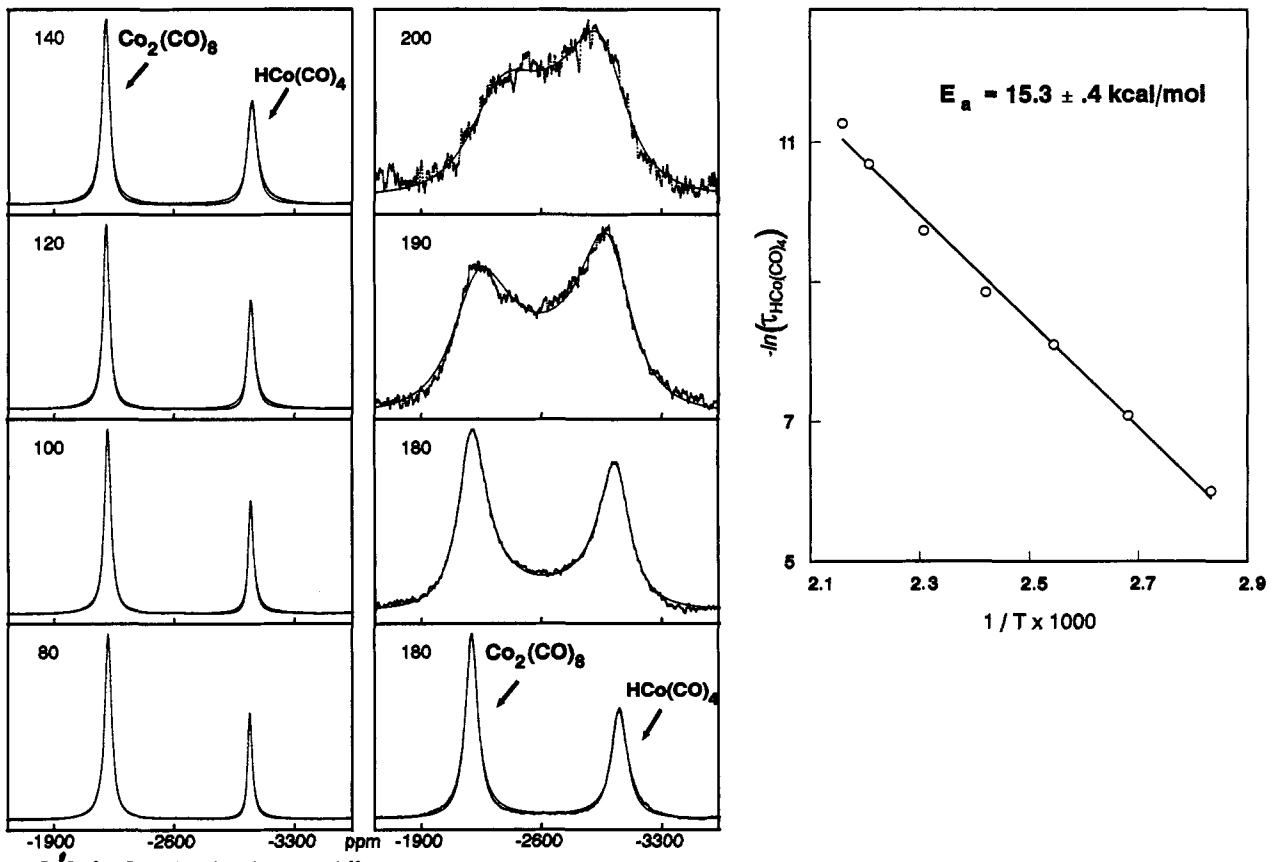

Figure 5. Left: Calculated and observed ^{59}Co NMR line widths for the reaction of $Co_2(CO)_8$ with $HCo(CO)_4$. Right: Arrhenius plot for the cobalt center lifetime in $HCo(CO)_4$. Conditions are as in Figure 2.

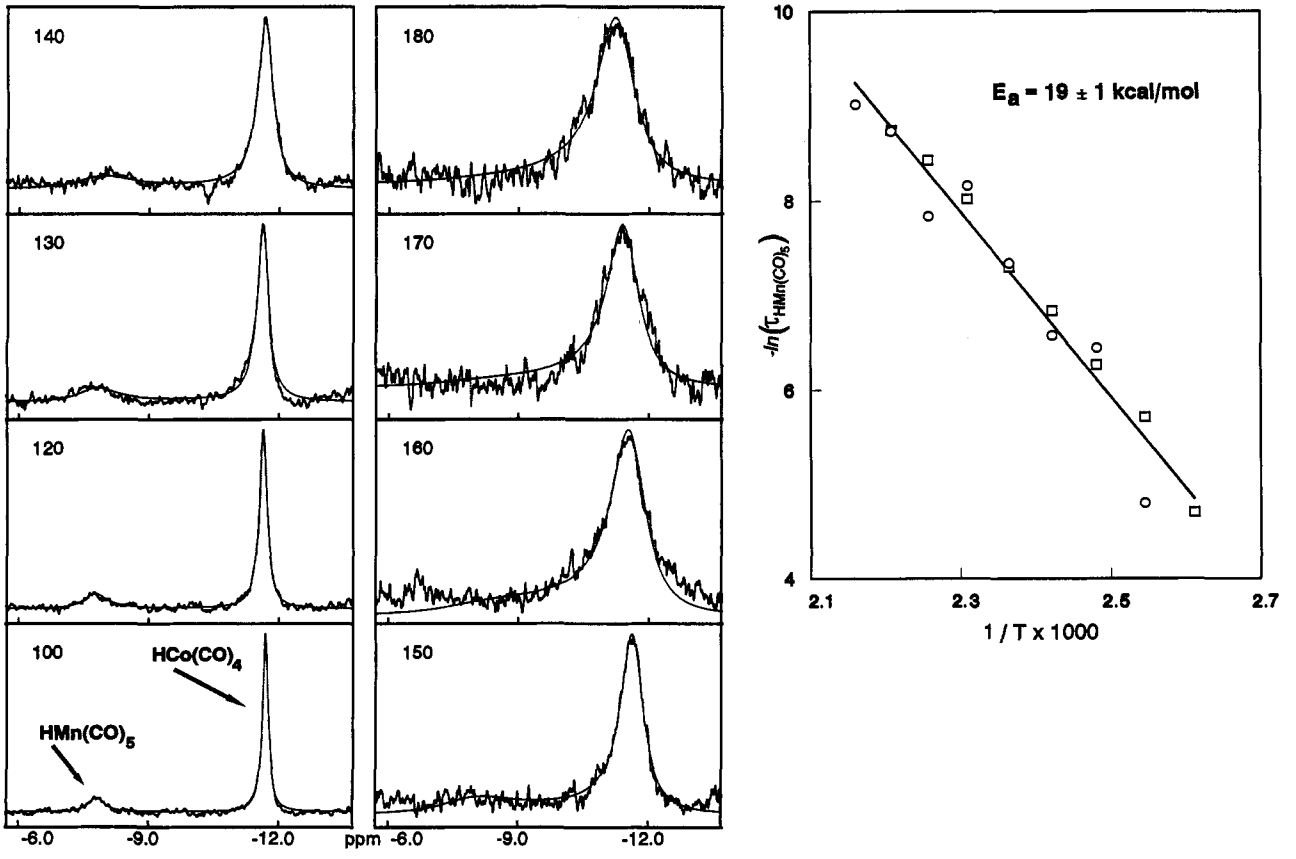

Figure 6. Left: Calculated and observed ^1H NMR for $HMn(CO)_5$ and $HCo(CO)_4$ under 1.4 M H_2 and 1.4 M CO. Right: Arrhenius plot for the Hydride lifetime in $HMn(CO)_5$. Key: ○, 4.13 M of CO; □, 1.39 M of CO.

transverse spin relaxation time, $T_2 = 1/\pi W_{1/2}$. In addition, all alternative reaction processes which similarly affect exchange between the manganese centers in $HMn(CO)_5$, $MnCo(CO)_9$, and $Mn_2(CO)_{10}$ are analogously ruled out on the time scale of the

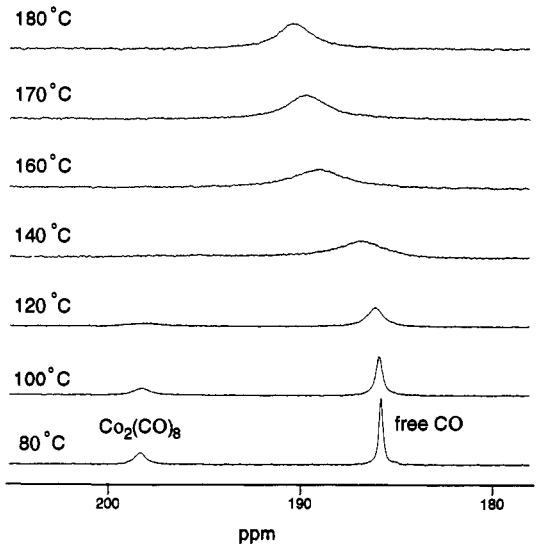

Figure 7. ^{13}C NMR spectra for CO exchange with $Co_2(CO)_8$ in mesitylene. Chemical shifts are relative to the unique aromatic solvent resonance at 137.4 ppm.

processes in eqs 6 and 7. A reasonable upper limit of 30 s^{-1} may be estimated for the rate of the manganese center exchange in eq 9 on the basis of eq 8 and a 10-Hz uncertainty in the natural ^{55}Mn line width ($W_{1/2}$) from Tables 5 and 6. Furthermore, the NMR magnetization transfer technique[21] is not expected to significantly lower the estimated upper limit of 30 s^{-1} for the exchange reaction in eq 9, as indicated by the T_1 measurements in the Experimental Section.

Thus, the cobalt center exchange in eq 6 occurs with an activation energy of 15.3 ± 0.4 kcal/mol. The heterometallic hydride ligand exchange in eq 7 is somewhat slower, with an activation energy of 19 ± 1 kcal/mol, and the manganese center exchange of eq 9 is too slow to measure by NMR transverse spin relaxation time measurements.

Carbonyl Exchange Reaction of $Co_2(CO)_8$. The kinetics of the ligand exchange reaction between the coordinated carbonyl groups in $Co_2(CO)_8$ and free carbon monoxide was studied between 40 and 80 °C by Roe using ^{13}C NMR magnetization transfer.[11] However, the industrial hydroformylation process is typically conducted at significantly higher temperatures.[1] Furthermore, at temperatures above 100 °C, the resonances for free and coordinated carbon monoxide broaden sufficiently that the peaks are no longer satisfactorily resolved to employ the magnetization transfer technique. Therefore, the $CO/Co_2(CO)_8$ ligand exchange system was analyzed by NMR line-shape analysis in the 100–180 °C range.

The stacked plot in Figure 7 shows that there is something unusual occurring in the $CO/Co_2(CO)_8$ exchange system. The resonances for free and coordinated carbon monoxide have merged by about 140 °C, yet this combined resonance continues to shift to lower fields as the temperature is increased. This temperature-dependent chemical shift is not due to changes in the relative equilibrium concentration of the bridging and terminal carbonyl groups[22] in $Co_2(CO)_8$ because the bridge–terminal equilibrium effect is small and can be quantitatively accounted for, as described in the Experimental Section. Furthermore, there were no unusual temperature-dependent chemical shifts or line broadenings observed for the mesitylene solvent. Therefore, the chemical shift

(21) (a) Muhandiram, D. R.; McClung, R. E. D. *J. Magn. Reson.* **1987**, *71*, 187–192. (b) Led, J. J.; Gesmar, H. *J. Magn. Reson.* **1982**, *49*, 444–463. (c) Roe, D. C. *J. Am. Chem. Soc.* **1983**, *105*, 7770–7771. (d) McKinney, R. J.; Roe, D. C. *J. Am. Chem. Soc.* **1986**, *108*, 5167–5173.

(22) (a) Hanson, B. E.; Sullivan, M. J.; Davis, R. J. *J. Am. Chem. Soc.* **1984**, *106*, 251–253. (b) Evans, J.; Johnson, B. F. G.; Lewis, J.; Matheson, T. W. *J. Am. Chem. Soc.* **1975**, *97*, 1245–1247. (c) Noack, K. *Helv. Chim. Acta* **1964**, *47*, 1064–1067. Noack, K. *Spectrochim. Acta* **1963**, *19*, 1925–1931.

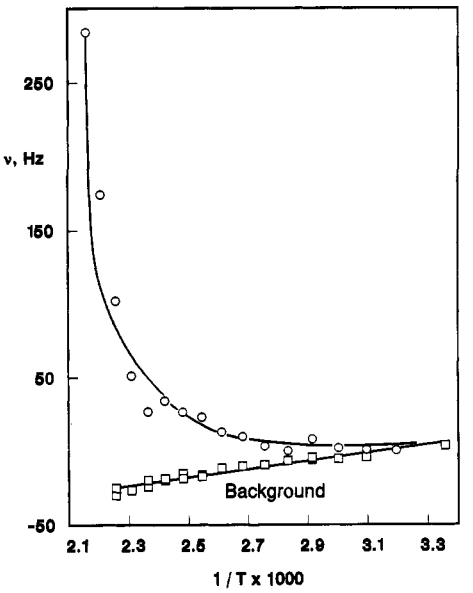

Figure 8. Chemical shift in the ^{13}C NMR spectrum for a mesitylene solution of CO in the absence, □, and presence, ○, of $Co_2(CO)_8$ at 0.117 M.

of the free carbon monoxide was treated as a refinable parameter during the least-squares fit to the two-site chemical exchange equilibrium of eq 10 for the spectral data in Figure 13 of the

$$Co_2(CO^*)_8 + CO \rightleftharpoons Co_2(CO^*)_7(CO) + CO^* \quad (10)$$

Experimental Section. There was minimal interaction between the refinable parameters in the least-squares fit, because the calculated line widths were affected mainly by the exchange lifetime while the location of the calculated resonance along the frequency axis was influenced predominately by the chemical shift for the free carbon monoxide. The resultant carbon monoxide chemical shift is plotted in Figure 8 along with the background dependence of the chemical shift for a mesitylene solution of carbon monoxide in the absence of $Co_2(CO)_8$.

Magnetic Susceptibility Measurements for $Co_2(CO)_8$. The thermolysis of the Co–Co bond in $Co_2(CO)_8$ changes the magnetic susceptibility of the solution due to the production of $^{\bullet}Co(CO)_4$ radicals. The extent of this dissociation was determined by measuring the temperature dependence of the volumetric susceptibility for a gas-phase solution of $Co_2(CO)_8$ in carbon monoxide by a modification of the Evan's NMR method[12] using methane as the reference peak in a small glass capillary as explained in the Experimental Section. The reference frequency difference, $\Delta\nu$, between the methane standard inside and outside of the capillary was monitored in the ^1H NMR spectra. This frequency difference responded reversibly to changes in the temperature over the range of 120 to 225 °C. Thus, $\Delta\nu$ decreased with an increase in the temperature, as expected for the production of a paramagnetic reaction product. Note that there is no contribution $\Delta\nu$ due to a temperature-dependent gas–liquid partition coefficient for the single-phase system employed in this NMR study. In addition, the density of a supercritical medium does not change with temperature. This contrasts to a liquid medium, where it is often necessary to correct the concentration data for changes in the density of the solvent.[12c]

The $^{\bullet}Co(CO)_4$ and the $Co_2(CO)_8$ concentrations were calculated from the reference frequency difference, $\Delta\nu$, as explained in the Experimental Section. The resultant temperature dependence for the equilibrium constant is given in the van't Hoff plot

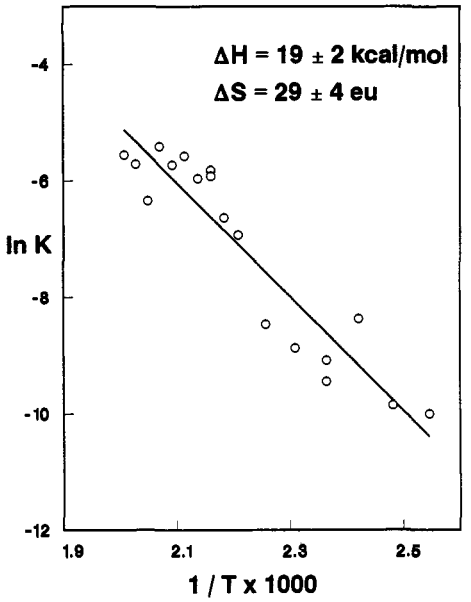

Figure 9. van't Hoff plot for Co–Co bond homolysis in $Co_2(CO)_8$ from magnetic susceptibility measurements.

of Figure 9. The entropy change is similar to the values found[23] for the dissociation of other metal dimers: $[\eta^3\text{-}C_3H_5Fe(CO)_3]_2$, 37 cal/(mol·K); $[\eta^5\text{-}C_5H_5Cr(CO)_3]_2$, 34–37 cal/(mol·K); $[\eta^5\text{-}C_5Me_5Cr(CO)_3]_2$, 45 cal/(mol·K). Furthermore, the dissociation entropy has now been measured for two series of related metal dimers, and it is reported[23a,f] that ΔS for M–M bond dissociation increases rapidly with the steric requirements of the ligands attached to the metal center. Consistently, ΔS for Co–Co bond dissociation in the simple carbonyl complex, $Co_2(CO)_8$, is lower than the values for the metal dimers listed above by an amount which is probably significant in comparison to the standard deviation in these measurements.

Discussion

The unusually facile exchange processes in eqs 6 and 7 raise anew an important mechanistic issue[24] with respect to the $Co_2(CO)_8$-catalyzed hydroformylation of olefins. What is the relative importance of oxidative addition pathways based on the coordinatively unsaturated $Co_2(CO)_7$ intermediate in comparison to alternative mechanistic pathways based on metal-centered radicals? Do both types of intermediates play a role in $Co_2(CO)_8$ catalysis? Indeed, it is the power of the recently developed *in situ* high-pressure NMR technique which allows the remarkably rapid chemical exchange processes in eqs 6 and 7 to be investigated in a direct manner. The speed of these exchange processes is dramatic in comparison to most of the reaction pathways that are of interest for oxo catalysis. Furthermore, the same highly reactive intermediate which is responsible for the exchange processes in eqs 6 and 7 may be an important factor in additional reaction pathways which involve dihydrogen or the olefin in oxo catalysis.

Mechanism for Hydride Ligand Exchange. The activation energy for the exchange of the cobalt centers in $HCo(CO)_4$ and $Co_2(CO)_8$ was determined by ^{59}Co NMR line-shape analysis, as indicated in Figure 5. This activation energy is lower[25] than those of all of the previous reports[10,11,26] for the activation barrier

Scheme 1. Proton Transfer

$$HCo(CO)_4 + H_2O \rightleftharpoons Co(CO)_4^- + H_3O^+ \quad (11)$$

$$HMn(CO)_5 + H_2O \rightleftharpoons Mn(CO)_5^- + H_3O^+ \quad (12)$$

net proton transfer

$$^*HCo(CO)_4 + H_2O \rightleftharpoons HCo(CO)_4 + H^*HO \quad (13)$$

Scheme 2. Oxidative Addition

$$Co_2(CO)_8 \rightleftharpoons Co_2(CO)_7 + CO \quad (14)$$

$$Co_2(CO)_7 + HMn(CO)_5 \rightleftharpoons [Co(CO)_4\text{-}HCo(CO)_3\text{-}Mn(CO)_5] \rightleftharpoons HCo(CO)_4 + CoMn(CO)_8 \quad (15)$$

$$CoMn(CO)_8 + CO \rightleftharpoons CoMn(CO)_9 \quad (16)$$

net oxidative addition

$$Co_2(CO)_8 + HMn(CO)_5 \rightleftharpoons MnCo(CO)_9 + HCo(CO)_4 \quad (17)$$

to carbonyl exchange in $Co_2(CO)_8$. These observations argue against a multistep reaction mechanism which includes carbonyl dissociation in eq 2 for the process by which the cobalt centers exchange in eq 6. A much stronger argument can be made on the basis of the mixed-metal system of eq 7. Three basic mechanistic possibilities exist for the hydride ligand exchange reaction between the manganese and cobalt centers of eq 7 and Figure 6 as indicated in Schemes 1–3.

The proton transfer mechanism of Scheme 1 is rapidly eliminated from consideration for the gas-phase system of eq 7 because there is no evidence for exchange of the hydride moieties with the proton centers in the water molecule on the time scale of the ^1H NMR observation. Thus, the water resonance remains a sharp distinct peak at 0.8 ppm in the ^1H NMR spectra; see Figure 4. In addition, the cobalt center exchange process in eq 6 cannot be explained solely on the basis of proton transfer.

Mechanistic variations based on oxidative-addition[8] processes deserve closer attention. Thus, the overall exchange process described by the stoichiometry in eq 17 of Scheme 2 is one such possibility. There are actually eight possible combinations for the oxidative addition mechanism in the $Mn_2(CO)_{10}/Co_2(CO)_8$ system, as summarized in Table 1. The reactions in eqs 14–16 provide more detail for the oxidative addition process in eq 17. A key step in this reaction process is the generation of a coordinatively unsaturated metal center by carbonyl dissociation, eq 14. Significantly, the oxidative addition process in eq 17 predicts that the manganese centers in $HMn(CO)_5$ and $MnCo(CO)_9$ must undergo exchange concurrent with the exchange of the hydride moieties between $HMn(CO)_5$ and $HCo(CO)_4$. Furthermore, all of the possible oxidative addition mechanisms which potentially result in transferring the hydride moiety from $HMn(CO)_5$ to $HCo(CO)_4$ (Schemes 2, 4, 9, and 10) require the concurrent exchange of the manganese center in $HMn(CO)_5$ with that in either $MnCo(CO)_9$ or $Mn_2(CO)_{10}$. In contrast, there is no evidence for exchange of these manganese centers on the time scale of the NMR observations, as demonstrated by the ^{55}Mn line-width data in Tables 5 and 6. Furthermore, the plot in Figure 10 demonstrates that exchange between the manganese centers in $HMn(CO)_5$, $MnCo(CO)_9$, and $Mn_2(CO)_{10}$ would be easily detected by ^{55}Mn NMR spectroscopy if it was indeed occurring at the same rate that the hydride ligand is observed to be exchanging in the ^1H NMR spectra. Thus, the simulated line width ($W_{1/2}$) in Figure 10 for the manganese center in $HMn(CO)_5$ was calculated according to the slow exchange approximation in eq 8 using the measured manganese hydride ligand lifetime from the ^1H NMR spectra in Figure 6.

(23) (a) Muetterties, E. L.; Sosinsky, B. A.; Zamaraev, K. I. *J. Am. Chem. Soc.* **1975**, *97*, 5299. (b) McLain, S. *J. Am. Chem. Soc.* **1988**, *110*, 643–644. (c) Goh, L. Y.; Hambley, T. W.; Darensbourg, D. J.; Reibenspies, J. *J. Organomet. Chem.* **1990**, *381*, 349–356. (d) Goh, L. Y.; Khoo, S. K.; Lim, Y. Y. *J. Organomet. Chem.* **1990**, *399*, 115–123. (e) Goh, L. Y.; Lim, Y. Y. *J. Organomet. Chem.* **1991**, *402*, 209. (f) Watkins, W. C.; Jaeger, T.; Kidd, C. E.; Fortier, S.; Baird, M. C.; Kiss, G.; Roper, G. C.; Hoff, C. D. *J. Am. Chem. Soc.* **1992**, *114*, 907–914.

(24) (a) Halpern, J. *Pure Appl. Chem.* **1986**, *58*, 575–584. (b) Orchin, M. *Ann. N.Y. Acad. Sci.* **1983**, *415*, 129–134.

(25) The plot in Figure 5 is based on the $HCo(CO)_4$ lifetime. Similarly, the activation enthalpy for cobalt center exchange based on the lifetime of a cobalt center in $Co_2(CO)_8$ is 17 kcal/mol. For comparison, measurements of the activation enthalpy for carbonyl exchange in $Co_2(CO)_8$ range from 18 to 25.5 kcal/mol, as summarized in Table 3 of the text.

(26) (a) Absi-Halabi, M.; Atwood, J. D.; Forbus, N. P.; Brown, T. *J. Am. Chem. Soc.* **1980**, *102*, 6249–6254. (b) Hoff, C. D.; Ungváry, F.; King, R. B.; Markó, L. *J. Am. Chem. Soc.* **1985**, *107*, 666–671.

Table 1. Exchange Process Based on a Oxidative-Addition Mechanism[a]

Scheme no.	CO loss[b]	metal hydride[c]	net exchange reaction
2[d]	Co	HMn	$Co_2(CO)_8 + HMn(CO)_5 \rightleftharpoons MnCo(CO)_9 + HCo(CO)_4$
4[d]	Co	HMn	$MnCo(CO)_9 + HMn(CO)_5 \rightleftharpoons Mn_2(CO)_{10} + HCo(CO)_4$
5	Co	HCo	$Co_2(CO)_8 + H^*Co(CO)_4 \rightleftharpoons Co^*Co(CO)_8 + HCo(CO)_4$
6	Co	HCo	$MnCo(CO)_9 + H^*CO(CO) \rightleftharpoons Mn^*Co(CO)_9 + HCo(CO)_4$
7	Mn	HMn	$Mn_2(CO)_{10} + H^*Mn(CO)_5 \rightleftharpoons Mn^*Mn(CO)_{10} + HMn(CO)_5$
8	Mn	HMn	$MnCo(CO)_9 + H^*Mn(CO)_5 \rightleftharpoons {}^*MnCo(CO)_9 + HMn(CO)_5$
9[d]	Mn	HCo	$Mn_2(CO)_{10} + HCo(CO)_4 \rightleftharpoons MnCo(CO)_9 + HMn(CO)_5$
10[d]	Mn	HCo	$MnCo(CO)_9 + HCo(CO)_4 \rightleftharpoons Co_2(CO)_8 + HMn(CO)_5$

[a] For mechanistic details, compare Scheme 2 in the text. [b] Metal center at which the open coordination site is created by carbonyl dissociation. [c] Metal hydride complex which adds to the open coordination site. [d] Process which results in hydride ligand transfer between the manganese and cobalt centers.

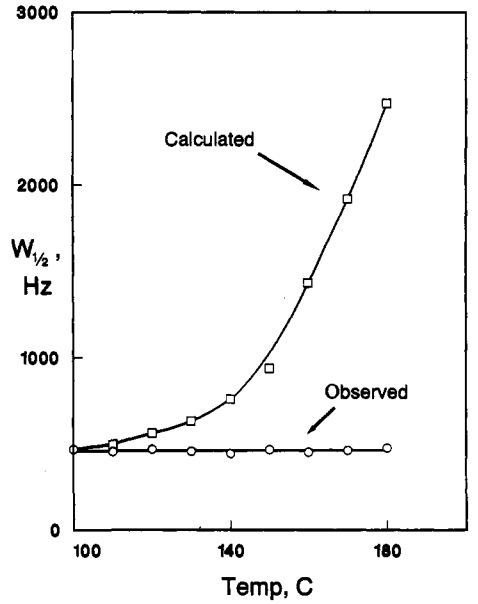

Figure 10. Observed, ○, and simulated, □, ^{55}Mn NMR line widths in $HMn(CO)_5$ based on the rate of hydride moiety exchange from the ^1H NMR spectra.

An additional argument exists against invoking the coordinatively unsaturated $Co_2(CO)_7$ species as a significant reaction intermediate for the exchange process in eq 7. Thus, there is no indication for inhibition by carbon monoxide in the hydride ligand exchange reaction of eq 7, as demonstrated in Figure 6.

The analysis of the oxidative-addition mechanism in Scheme 2 critically depends on the absence of measurable exchange between $HMn(CO)_5$, $Mn_2(CO)_{10}$, and $MnCo(CO)_9$ in the ^{55}Mn NMR spectra. Significantly, the calculation for Figure 10 does not rule out all potential manganese-containing intermediates for the hydride ligand exchange reaction in eq 7. The plot in Figure 10 only rules out those manganese-containing intermediates which are present at sufficiently high concentration levels that they are visible as discrete resonances in the ^{55}Mn NMR spectra. One possible intermediate which is present at concentration levels well below those that can be directly detected in the ^{55}Mn NMR spectra is a $^*Mn(CO)_5$ radical. The proposed mechanism in Scheme 3 for the hydride ligand exchange reaction in eq 7 is based on a $^*Mn(CO)_5$ radical intermediate. The central chain propagation steps of the hydrogen atom transfer process in eqs 19 and 20 of Scheme 3 do not contain $MnCo(CO)_9$ or $Mn_2(CO)_{10}$. Therefore, the hydrogen atom transfer mechanism provides a pathway for exchanging the hydride moiety between the manganese and cobalt centers in $HMn(CO)_5$ and $HCo(CO)_4$ which does not require concurrent exchange of the manganese centers in $HMn(CO)_5$, $MnCo(CO)_9$, and $Mn_2(CO)_{10}$ as summarized in the overall stoichiometry in eq 23. Furthermore, a potential $^*Mn(CO)_5$ radical intermediate should have a minimal effect on the $HMn(CO)_5$ line width in the ^{55}Mn NMR spectra, as elaborated in the Experimental Section.

Scheme 3. Hydrogen Atom Transfer

initiation

$$Co_2(CO)_8 \overset{K_d}{\rightleftharpoons} 2\cdot Co(CO)_4 \quad (18)$$

propagation

$$HMn(CO)_5 + \cdot Co(CO)_4 \xrightarrow{k_{19}} \cdot Mn(CO)_5 + HCo(CO)_4 \quad (19)$$

$$HCo(CO)_4 + \cdot Mn(CO)_5 \xrightarrow{k_{20}} \cdot Co(CO)_4 + HMn(CO)_5 \quad (20)$$

termination

$$2\cdot Mn(CO)_5 \longrightarrow Mn_2(CO)_{10} \quad (21)$$

$$\cdot Mn(CO)_5 + \cdot Co(CO)_4 \longrightarrow MnCo(CO)_9 \quad (22)$$

net radical chain

$$^*HMn(CO)_5 + HCo(CO)_4 \rightleftharpoons HMn(CO)_5 + {}^*HCo(CO)_4 \quad (23)$$

Activation Barriers in Hydrogen Atom Transfer. The mechanism in Scheme 3 indicates that the activation parameters in Figures 5 and 6 contain a combination of Co–Co bond homolysis and hydrogen atom transfer terms. However, these two kinetic processes can be resolved. The analysis of the kinetics for the hydrogen atom transfer mechanism of Scheme 3 is simplified if it can be assumed that the chain termination step in eq 22 will not significantly perturb the equilibrium $^*Co(CO)_4$ concentration based on $Co_2(CO)_8$ dissociation in eq 18. Assumption of a steady state in the $^*Co(CO)_4$ radical concentration provides eq 24, which

$$[^*Co(CO)_4] = K_d^{1/2}[Co_2(CO)_8]^{1/2} \quad (24)$$

yields the rate law in eq 25 for the hydrogen atom transfer process in eq 19. The result in eq 25 indicates that the second-order rate

$$-\frac{d[HMn(CO)_5]}{dt} = k_{19}K_d^{1/2}[HMn(CO)_5][Co_2(CO)_8]^{1/2} \quad (25)$$

constants for hydrogen atom transfer, k_{19}, may be calculated from the $HMn(CO)_5$ lifetimes in Figure 6 and the $Co_2(CO)_8$ concentrations according to the expression in eq 26. The required

$$k_{19} = (\tau_{HMn(CO)_5})^{-1}K_d^{-1/2}[Co_2(CO)_8]^{-1/2} \quad (26)$$

Co–Co bond homolysis constants, K_d, were obtained from the thermodynamics in Figure 9. The quantitative analysis of hydrogen atom transfer in the cobalt system of eq 27 is somewhat

$$HCo(CO)_4 + {}^*Co(CO)_4 \rightleftharpoons {}^*Co(CO)_4 + HCo(CO)_4 \quad (27)$$

more complex in that the $^*Co(CO)_4$ radical itself can potentially add to the observed ^{59}Co NMR line widths. Thus, implicit to the two-site exchange simulation of Figure 5 is the underlying assumption that the chemical shift of the $^*Co(CO)_4$ radical is sufficiently large that this species is not in fast exchange with

$Co_2(CO)_8$ or $HCo(CO)_4$ on the ^{59}Co NMR time scale. Consistently, the finial hydrogen atom transfer rate constants obtained for eq 27 agree to within 1 order of magnitude with those for eq 19 which were obtained from the ^1H NMR data of Figure 6 where it is not necessary to make assumptions regarding the $^{\bullet}Co(CO)_4$ radical. Thus, the $HCo(CO)_4$ lifetimes from Figure 5 yield the second-order rate constants for the degenerate hydrogen atom transfer reaction in eq 27 according to the expression in eq 28. These second-order rate constants for the degenerate hydrogen

$$k_{27} = (\tau_{HCo(CO)_4})^{-1}K_d^{-1/2}[Co_2(CO)_8]^{-1/2} \quad (28)$$

atom transfer reaction in eq 27 range from 1.1×10^6 M^{-1} s^{-1} at 80 °C to 1.1×10^7 M^{-1} s^{-1} at 190 °C and yield activation parameters of $\Delta H^{\ddagger} = 5.5 \pm 0.6$ kcal mol^{-1} and $\Delta S^{\ddagger} = -16 \pm 4$ cal mol^{-1} deg^{-1}. Hydrogen atom transfer in the mixed-metal system of eq 19 is slower by approximately 1 order of magnitude yielding activation parameters of $\Delta H^{\ddagger} = 10 \pm 1$ kcal mol^{-1} and $\Delta S^{\ddagger} = -8 \pm 2$ cal mol^{-1} deg^{-1}.

The termination steps of the hydrogen atom transfer mechanism in Scheme 3 deserve comment on two points. First, the competition between the reactions in eqs 20 and 22 determines the chain length or how many times the hydride moiety exchanges between the $HMn(CO)_5$ and $HCo(CO)_4$ complexes (greater than 10^4 transfers per second at 190 °C) before an exchange of the manganese center occurs between the $HMn(CO)_5$ and $MnCo(CO)_9$ species (less than 30 transfers per second). The observed chain length is consistent with our expectations because both the radical dimerization process in eq 22 and the thermodynamically favorable hydrogen atom transfer process in eq 20 are likely to proceed at rates near the diffusion limit. Thus, even the degenerate hydrogen atom transfer reaction in eq 27 proceeds with second-order rate constants of 10^6–10^7 M^{-1} s^{-1}. These values are to be compared with the rate constant[9b] for $^{\bullet}Co(CO)_4$ dimerization of 4×10^8 M^{-1} s^{-1}. Furthermore, the reaction in eq 20 is thermodynamically favorable by as much as 10 kcal mol^{-1} and is likely to have a smaller activation barrier than the reaction in eq 27. Therefore, if both the reactions in eqs 20 and 22 occur at rates near the diffusion limit, then the length of the radical chain will be determined by the concentration ratio of $HCo(CO)_4$ to $^{\bullet}Co(CO)_4$, which is greater than 10^2 even at 200 °C. Second, on the basis of the second-order rate constant measurements for the reactions in eqs 19 and 27, the analogous degenerate hydrogen atom transfer reaction in eq 29 is also likely to be quite

$$HMn(CO)_5 + {}^{\bullet}Mn(CO)_5 \rightleftharpoons {}^{\bullet}Mn(CO)_5 + HMn(CO)_5 \quad (29)$$

fast. However, the manganese center exchange reaction in eq 9 is too slow to observe by line width (T_2) measurements. Therefore, these two observations indicate that the radical recombination step as written in eq 21 must be effectively irreversible on the time scale of the ^{55}Mn NMR measurements. Consistently, the Mn–Mn BDE in $Mn_2(CO)_{10}$ is approximately 38 kcal/mol as recently reviewed.[27] Similarly, the sharpness of the $MnCo(CO)_9$ resonance in the ^{59}Co NMR spectra, under conditions where the peaks for $HCo(CO)_4$ and $Co_2(CO)_8$ have merged, suggests that the radical recombination reaction in eq 22 is also effectively irreversible on the ^{59}Co NMR time scale.

The significant difference in the chemical exchange line broadening of the $MnCo(CO)_9$ and $Co_2(CO)_8$ resonances in the ^{59}Co NMR spectra suggests a large difference in the Mn–Co and the Co–Co BDE. In addition, the Mn–Co BDE is close to the average of the Mn–Mn and Co–Co values because the equilibrium constant for the disproportionation reaction in eq 30 is close to unity.[15] This question of the relative magnitude for the Mn–Mn and Co–Co BDE is addressed in greater detail in the next section.

$$Mn_2(CO)_{10} + Co_2(CO)_8 \rightleftharpoons 2MnCo(CO)_9 \quad (30)$$

Co–Co and Co–H Bond Dissociation Enthalpies. The activation enthalpy for hydrogen atom transfer in the mixed-metal system of eq 19 is related to the difference in metal–hydrogen bond enthalpies according to eq 31, where $\Delta H_{20}^{\ddagger}$ is the residual

$$\Delta H_{19}^{\ddagger} = BDE(Mn\text{–}H) - BDE(Co\text{–}H) + \Delta H_{20}^{\ddagger} \quad (31)$$

activation enthalpy for hydrogen atom transfer in the thermodynamically favorable direction of eq 20. In addition, the Co–Co BDE for $Co_2(CO)_8$ is related to the Co–H BDE on the basis of the measured enthalpy of hydrogenation[13,14] in eq 4 and a H–H BDE in H_2 of 104 kcal/mol according to eq 32. The corresponding result from the manganese hydrogenation[15,28] in eq 5 is given in eq 33.

$$\Delta H_d = BDE(Co\text{–}Co) = 2BDE(Co\text{–}H) - 99.3 \text{ kcal} \quad (32)$$

$$BDE(Mn\text{–}Mn) = 2BDE(Mn\text{–}H) - 95.3 \text{ kcal} \quad (33)$$

The cobalt BDE values result directly. Thus, the Co–Co BDE was independently determined by magnetic susceptibility measurements in Figure 9. The measured Co–Co BDE was used in conjunction with eq 32 to calculate the Co–H BDE. The resultant cobalt BDE values are included in the last column of Table 2. Consistently, the activation enthalpy for degenerate hydrogen atom transfer between $HCo(CO)_4$ and $^{\bullet}Co(CO)_4$ for the reaction in eq 27 is 9.3% of the Co–H BDE, which is within the 5–10% range predicted by the theory developed by Marcus[29] for atom transfer reactions. In addition, the activation entropy ($\Delta S_{27}^{\ddagger} = -16$ cal mol^{-1} deg^{-1}) for the degenerate hydrogen atom transfer process in eq 27 is close in absolute value to the dissociation entropy for $Co_2(CO)_8$ in Figure 9 and is consistent with a dimeric Co–H–Co transition state. A negative activation entropy ($\Delta S^{\ddagger} = -38$ cal mol^{-1} deg^{-1}) also has been reported for hydrogen atom transfer in the $[\eta^5\text{-}C_5Me_5Cr(CO)_3]_2$ system.[30] Negative activation entropies have been reported[31a] and used[31b] for other atom transfer reactions involving organometals. Comparable values have been reported for proton transfer processes.[32]

Table 2. Bond Dissociation Enthalpies Based on Hydrogen Atom Transfer Kinetics

BDE	upper limit,[a] kcal	estimate,[b] kcal	measd,[c] kcal
Mn–H	69	66 ± 2	*d*
Mn–Mn	44	38 ± 4	*d*
Co–H	*d*	*d*	59[e] ± 1
Co–Co	*d*	*d*	19 ± 2

[a] Calculated from eqs 26 and 32 in the text, assuming no activation enthalpy for hydrogen atom transfer in the thermodynamically favorable direction of eq 20. [b] Based on an estimated enthalpic barrier of 3 ± 2 kcal for the reaction in eq 20. [c] Measured from the magnetic susceptibility in Figure 9. [d] Not determined. [e] Calculated with eq 32 and the measured Co–Co BDE of 19 ± 2 kcal.

(27) (a) Martinho Simões, J. A.; Beauchamp, J. L. *Chem. Rev.* **1990**, *90*, 629. (b) Goodman, J. L.; Peters, K. S.; Vaida, V. *Organometallics* **1986**, *5*, 815–816. (c) Pugh, J. R.; Meyer, T. J. *J. Am. Chem. Soc.* **1992**, *114*, 3784–3792. (d) Martinho Simões, J. A.; Schultz, J. C.; Beauchamp, J. L. *Organometallics* **1985**, *4*, 1238–1242.

(28) Kiss, G.; Nolan, S. P.; Hoff, C. D. Private communication.

(29) (a) Marcus, R. A. *J. Phys. Chem.* **1968**, *72*, 891–899. (b) Cohen, A. O.; Marcus, R. A. *J. Phys. Chem.* **1968**, *72*, 4249–4256.

(30) Kiss, G.; Zahang, K.; Mukerjee, S. L.; Hoff, C. D. *J. Am. Chem. Soc.* **1990**, *112*, 5657–5658.

(31) (a) Eisenberg, D. C.; Lawrie, C. J. C.; Moody, A. E.; Norton, J. R. *J. Am. Chem. Soc.* **1991**, *113*, 4888–4895. (b) Song, J. S.; Bullock, R. M.; Creutz, C. *J. Am. Chem. Soc.* **1992**, *113*, 9862–9864. (c) Lee, K.; Brown, T. L. *J. Am. Chem. Soc.* **1987**, *109*, 3269–3275.

(32) (a) Edidin, R. T.; Sullivan, J. M.; Norton, J. R. *J. Am. Chem. Soc.* **1987**, *109*, 3945–3953. (b) Creutz, C.; Sutin, N. *J. Am. Chem. Soc.* **1988**, *110*, 2418–2427. (c) Kristjánsdóttir, S. S.; Norton, J. R. *J. Am. Chem. Soc.* **1991**, *113*, 4366–4367.

Strict upper limits for the Mn–Mn and Mn–H BDE values may be calculated from eqs 31–33 by assuming that the residual barrier to hydrogen atom transfer for the reaction in eq 20 is zero. These limits are listed in column 2 of Table 2. Although the residual barrier for hydrogen atom transfer in eq 20 will not be zero, this barrier is expected to be small. Thus, the intrinsic activation barrier for the degenerate atom transfer process in eq 27 is 5.5 kcal mol^{-1}. Furthermore, the Marcus theory indicates that the activation barrier will decrease for exothermic atom transfer processes. An enthalpic barrier of 2.1 kcal/mol has been reported[30] for an exothermic hydrogen atom transfer reaction between two chromium metal centers. Therefore, reasonable estimates for $\Delta H_{20}^{\ddagger}$ range from 2 to 5 kcal/mol. This range of estimated values was used to calculate the manganese BDE values in column 3 of Table 2. Note that the manganese BDE parameters in columns 2 and 3 of Table 2 are nearly independent[33] of the value used for the Co–Co bond dissociation enthalpy, ΔH_d.

It has not been possible to similarly measure the $\cdot Mn(CO)_5$ radical concentration by magnetic susceptibility measurements below 250 °C, consistent with the estimated strength of the Mn–Mn bond in column 3 of Table 2. Furthermore, the values in Table 2 are comparable to existing literature values. Tilset and Parker report[34] a Mn–H BDE of 68 kcal/mol based on a pK_a and electrochemical technique. This value is close to the upper limit in column 2 of Table 2. Alternatively, a lower literature value of 62 kcal/mol exists for the Mn–H BDE. This value is based on the kinetics of hydrogen atom transfer to olefinic substrates.[35] The estimated Mn–H BDE in Table 2 is consistent with either of these literature values (68 or 62 kcal/mol) to within the uncertainty for $\Delta H_{20}^{\ddagger}$ in eq 31. Similarly, there exist a range of literature values for the Mn–Mn BDE, extending from 19 to 42 kcal/mol. However, as reviewed elsewhere,[27a] recent mass spectroscopic and photoacoustic calorimetric measurements concur[27] that the Mn–Mn BDE is approximately 38 ± 5 kcal/mol, which agrees with the NMR value in column 3 of Table 2.

The situation with respect to the important oxo catalyst is not as favorable. The Co–Co BDE from mass spectroscopy[27a,36] (15 kcal/mol) is lower than the (magnetic susceptibility based) enthalpy result in column 4 of Table 2 by an amount which is outside the standard deviation in the two measurements. An additional inconsistency exists with respect to the Co–H bond. Thus, the Co–H BDE value based on p$K_a/E°$ measurements[34] is 67 kcal/mol. This p$K_a/E°$ value is significantly higher[37] than the NMR result in column 4 of Table 2. Fortunately, there is a third experimental approach. Thus, an upper limit of 63 kcal/mol is obtained[9a] for the Co–H BDE on the basis of the activation parameters for $\cdot H$ transfer to styrene.[38] Consistently, the NMR determination for the Co–H BDE in the last column of Table 2 is below this estimated upper limit of 63 kcal/mol.

The different Co–Co BDE values determined by mass spectroscopy (15 kcal/mol) and magnetic susceptibility (19 kcal/mol) translate into measurably different $\cdot Co(CO)_4$ concentrations when they are used to calculate the equilibrium constant for the dissociation of $Co_2(CO)_8$ in eq 18 (or eq 1). Thus, at an initial $Co_2(CO)_8$ loading of 0.018 M, the magnetic susceptibility data in Figure 9 suggests that $Co_2(CO)_8$ is 2% dissociated at 150 °C, while the mass spectroscopically determined Co–Co BDE predicts 37% dissociation. Significantly, the Co–Co bond in $Co_2(CO)_8$ appears to be sufficiently weak that the $\cdot Co(CO)_4$ radical may be investigated by several complementary NMR techniques as discussed in the following sections. These additional experimental methods serve to corroborate the Co–Co and Co–H BDE values listed in column 4 of Table 2.

Table 3. Summary of Activation Parameters for Carbonyl Exchange in $Co_2(CO)_8$

technique	temp range, °C	$\Delta H^{\ddagger}$, kcal	$\Delta S^{\ddagger}$, eu
^{14}C tracer[a]	−20 to 5	21 ± 2	5 ± 4
ligand sub[b]	15 to 30	22 ± 1	6 ± 2
NMR, mag tran[c]	40 to 80	25.5 ± 1.5	22 ± 4
NMR, line shape[d]	80 to 180	18 ± 2	3 ± 2

[a] By ^{14}CO tracer methods in toluene solvent; calculated from the rate constants in ref 10. [b] By $AsPh_3$ ligand substitution kinetics in hexane solvent; calculated from the rate constants in ref 26a. [c] By ^{13}C NMR magnetization transfer in cyclohexane-d_{12} solvent from ref 11. [d] By ^{13}C NMR line-shape analysis is mesitylene solvent from Figure 13.

Contact Shift for CO with $Co_2(CO)_8$. The rate of carbonyl exchange in the $Co_2(CO)_8$ system was originally investigated by Basolo and Wojcicki[10] using ^{14}C tracer methods. This carbonyl exchange problem was readdressed by Brown[26a] using ligand substitution and later by Roe[11] using a ^{13}C NMR magnetization transfer technique. The ^{13}C NMR line-width analysis of Figure 13 in the experimental section extends the range of temperatures that have been investigated for the rate of carbonyl exchange in $Co_2(CO)_8$ into the region that is used for the industrial hydroformylation process. All of the techniques yield similar activation enthalpies, as summarized in Table 3. Some of the scatter evident in the data of Table 3 may be due to the different solvents that were used in these investigations. Furthermore, the general agreement between the experimental methods in Table 3 is quite good because all of the original rate constant data may be collectively fit with a single line (correlation coefficient of 0.996) in an Arrhenius plot that covers a range of approximately 10 orders of magnitude in rate constants and temperatures from −20 to 180 °C.

Significantly, at the elevated temperatures employed during the NMR line-shape analysis, the carbon monoxide was observed to exhibit a large temperature-dependent chemical shift, as demonstrated in Figure 8. This unusual chemical shift dependence is interpreted as a contact shift brought about by the interaction of the carbon monoxide ligand with a paramagnetic metal center whose concentration increases exponentially with temperature. The most likely paramagnetic metal center in the system is the $\cdot Co(CO)_4$ radical, which is produced by Co–Co bond homolysis in eq 18 (or eq 1). In addition, it is possible that the $\cdot Co(CO)_4$ radical subsequently reacts with carbon monoxide to yield $\cdot Co(CO)_5$ or the aromatic solvent to yield a π-complex. However, there is no direct spectroscopic evident to invoke 19-electron cobalt complexes. Thus, the analysis of the rate of Co–Co bond homolysis by ^{59}Co NMR line width analysis in Figure 12 of the next section gives a result that is consistent with the magnetic susceptibility value in Figure 9. This agreement between kinetic and equilibrium thermodynamic determinations for the Co–Co BDE argues against significant levels of $\cdot Co(CO)_5$ complex formation under these reaction conditions. In addition, no unusual internal chemical shifts were noted for the mesitylene solvent which correspondingly argues against extensive complex formation between the cobalt radical and the aromatic solvent. In the following analysis of the contact shift data, it is assumed that $\cdot Co(CO)_4$ is the major cobalt radical species in the system. Contact shifts have been extensively

(33) If the $Co_2(CO)_8$ concentration was completely independent of temperature, then the calculated Mn–H BDE would be independent of the value used for ΔH_d. In this later case, the resultant Mn–H BDE would depend only on the slope of the plot in Figure 6 and the measured thermodynamics for the hydrogenation reaction in eq 5. The $Co_2(CO)_8$ concentrations do vary somewhat with temperature due to the equilibrium processes in eqs 1 and 4. As a measure of the magnitude of this approximation, the resultant activation enthalpy $\Delta H_{19}^{\ddagger}$ obtained by using an average $Co_2(CO)_8$ concentration is 9.5 kcal mol^{-1}, which compares favorably with the result in the text of 10 kcal mol^{-1} obtained by using the actual $Co_2(CO)_8$ concentration at each temperature.

(34) (a) Tilset, M.; Parker, V. D. *J. Am. Chem. Soc.* **1989**, *111*, 6711–6717. (b) Tilset, M.; Parker, V. D. *J. Am. Chem. Soc.* **1990**, *112*, 2843.

(35) (a) Bilmers, R.; Griffith, L. L.; Stein, S. E. *J. Phys. Chem.* **1986**, *90*, 517–523. (b) Sweany, R. L.; Halpern, J. *J. Am. Chem. Soc.* **1975**, *97*, 7186.

(36) (a) Bidinosti, D. R.; McIntyre, N. S. *J. Chem. Soc., Chem. Commun.* **1967**, 1. (b) Bidinosti, D. R.; McIntyre, N. S. *Can. J. Chem.* **1970**, *48*, 593–597.

(37) The 8 kcal/mol discrepancy is not improved by using the mass spectroscopically determined value for the Co–Co BDE in eq 32. In that case, the p$K_a/E°$ value for the Co–H BDE is 10 kcal/mol higher than the Co–H BDE from eq 32.

(38) Ungváry, F.; Markó, L. *Organometallics* **1982**, *1*, 222.

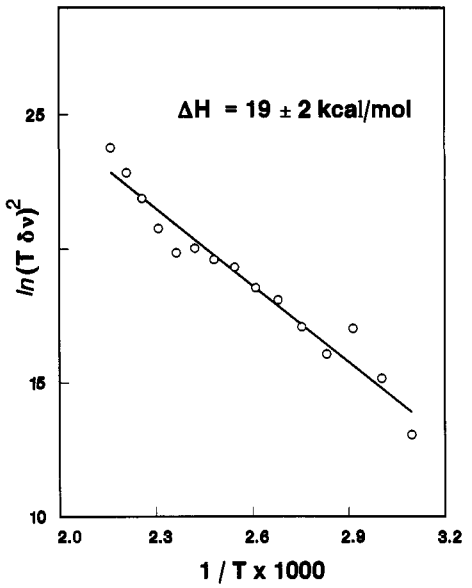

Figure 11. Co–Co bond dissociation energy of $Co_2(CO)_8$ from the contact shift for CO in the ^{13}C NMR spectra.

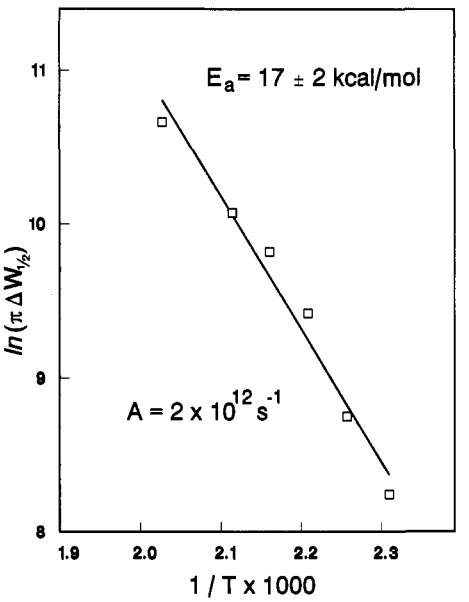

Figure 12. Arrhenius plot for Co–Co bond homolysis in $Co_2(CO)_8$ based on the ^{59}Co NMR line widths.

studied for oxygen donor ligands in aqueous systems, where a variety of labile paramagnetic metal centers are available for study.[39] Similarly, if the carbonylx ligands in the $\cdot Co(CO)_4$ radical are in fast exchange with the free ligand, then the observed frequency will be equal to the weighted average according to eq 34, where f is the mole fraction of the carbon monoxide in the

$$\nu_{obs} = (1-f)\nu_{CO} + f\nu_{radical} \quad (34)$$

$\cdot Co(CO)_4$ radical. Furthermore, the quantity $(1-f)$ cannot differ substantially from unity with a large excess of free carbon monoxide, so that the change in the chemical shift, $\delta\nu = \nu_{obs} - \nu_{CO}$, is proportional to $f\nu_{radical}$. In addition, the ^{13}C chemical shift of the $\cdot Co(CO)_4$ radical is inversely proportional to the temperature[17a,39] according to eq 35, in the absence of significant

$$\nu_{radical} \propto \left(\frac{\Delta H}{H_0}\right)_i = -\frac{g_e\beta_e}{g_N\beta_N}\frac{A_i S(S+1)}{3kT} \quad (35)$$

dipolar contributions where A_i is the isotropic hyperfine coupling constant. Therefore, eqs 34 and 35 indicate that the mole fraction f and, similarly, the concentration of the $\cdot Co(CO)_4$ radical should be proportional to $\delta\nu T$. Furthermore, the equilibrium constant for Co–Co bond homolysis in eq 18 (or eq 1) will be proportional to the square of the radical concentration at low percent conversions. Accordingly, the temperature dependence of the contact shift in Figure 8 provides a 19 ± 2 kcal/mol estimate for the Co–Co BDE, as shown in Figure 11. This result compares favorably with the value determined by magnetic susceptibility measurements in Figure 9.

The analysis of the temperature-dependent chemical shift in Figure 8 as a contact shift requires that some of the carbonyl exchange in the $Co_2(CO)_8$ system proceeds through a $\cdot Co(CO)_4$ radical intermediate. However, the $\cdot Co(CO)_4$-based carbonyl exchange route is not required to be the major mechanistic pathway. Indeed, previous investigations of the mechanism for carbonyl exchange in $Co_2(CO)_8$ conclude[10,11,26] that the reaction proceeds through the coordinatively unsaturated $Co_2(CO)_7$ intermediate of eq 2. The most compelling observation is stepwise ligand substitution[26a] in $Co_2(CO)_8$ with $AsPh_3$. Therefore, the available evidence is best explained by assuming that the primary pathway for carbonyl exchange in $Co_2(CO)_8$ proceeds through the coordinatively unsaturated $Co_2(CO)_7$ intermediate, with an alternative carbonyl exchange pathway based on $\cdot Co(CO)_4$ radicals lying close in energy.[40]

The contact chemical shift data in Figure 11 and magnetic susceptibility measurements in Figure 9 indicate that approximately 2% of the $Co_2(CO)_8$ is dissociated at 150 °C and an initial $Co_2(CO)_8$ loading of 0.018 M. Therefore, the ^{59}Co NMR line width for the $Co_2(CO)_8$ complex must correspondingly respond,[20] even in the absence of dihydrogen, to the dynamics of the dissociation process in eq 18 (or eq 1). Furthermore, the $\cdot Co(CO)_4$ radical concentrations should be well above the level necessary to employ the slow exchange approximation of eq 8 in calculating the rate constant for cobalt bond homolysis in $Co_2(CO)_8$, as explained in the discussion of eqs 40–42 in the Experimental Section. The resultant Arrhenius plot in Figure 12, derived from the data in Figure 1, provides a consistent activation energy and a reasonable frequency factor[41] from the slope and intercept, respectively.

$\cdot Co(CO)_4$ Radicals in Oxo Catalysis. The existence of thermally generated $\cdot Co(CO)_4$ radicals under hydroformylation reaction conditions is unequivocally demonstrated by the hydrogen atom transfer reactions of eqs 6 and 7. Furthermore, the level of activity due to the equilibrium $\cdot Co(CO)_4$ radical concentration is quite pronounced. Thus, the exchange of the hydride moiety between the cobalt centers in $HCo(CO)_4$ and $Co_2(CO)_8$ is occurring more than a million times faster than the steady-state rate of transfer for the same hydride moiety to the olefin in the hydroformylation process.[4] The NMR methods summarized in Table 4 indicate that the Co–Co BDE is quite similar to the activation enthalpy for carbonyl exchange in $Co_2(CO)_8$, as listed in Table 3. Therefore, $\cdot Co(CO)_4$ radical formation competes effectively with carbonyl dissociation from the oxo catalyst, $Co_2(CO)_8$.

One of the most intriguing aspects of the hydroformylation reaction is that dihydrogen is consumed faster than the initial rate at which $Co_2(CO)_8$ is hydrogenated in the absence of the

(39) (a) Eaton, D. E.; Philips, W. D. *Adv. Magn. Reson.* **1965**, *1*, 103–148. (b) Jesson, J. P. In *NMR of Paramagnetic Molecules*; La Mar, G. N., Horrocks, W. DeW., Holm, R. H., Eds.; Academic Press: New York, 1973; p 11.

(40) The enthalpic barrier for the $\cdot Co(CO)_4$-based carbonyl exchange pathway in $Co_2(CO)_8$ will be equal to the sum of half the Co–Co BDE (19 kcal/mol from Table 4) and the enthalpic barrier for carbonyl exchange in the $\cdot Co(CO)_4$ radical. This is to be compared with ΔH^* for the $Co_2(CO)_7$-based carbonyl exchange pathway in Table 3 of 18–25 kcal/mol. Therefore, the enthalpic barrier for carbonyl exchange in the $\cdot Co(CO)_4$ radical is indicated to be greater than 8.5 kcal/mol. Furthermore, the carbonyl exchange barrier in the $\cdot Co(CO)_4$ radical must be less than 18–25 kcal/mol, because the $\cdot Co(CO)_4$ radical is in fast exchange with the free carbon monoxide at 80–120 °C, where the $Co_2(CO)_8$/CO exchange is still in the slow exchange region.

(41) Reference 19, Chapter 8.

Table 4. NMR Estimates for the Energetics of $^{\bullet}Co(CO)_4$ Radical Formation

technique	solvent	Co–Co BDE, kcal
magnetic susceptibility[a]	CO	19 ± 2
^{13}CO contact chem shift[b]	mesitylene	19 ± 2
^{59}Co line widths[c]	CO_2	17 ± 2
hydrogen atom transfer and Marcus theory[d]	CO_2	19 ± 2

[a] From the magnetic susceptibility data in Figure 9. [b] From the ^{13}CO contact chemical shift data in Figure 11. [c] From the ^{59}Co NMR linewidth data for $Co_2(CO)_8$ in Figure 12. [d] From eqs 28 and 32 in addition to the prediction from the Marcus theory that the intrinsic barrier to hydrogen atom transfer, $\Delta H^{\ddagger}$, will be 5–10% of the Co–H BDE.

olefin.[1,2,4,6] Therefore, we are currently looking for reactions of the type[42] in eq 36. The proposed reaction in eq 36 may proceed

$$^{\bullet}Co(CO)_4 + H\text{–}H + CH_2{=}CHR \rightarrow HCo(CO)_4 + CH_3\dot{C}HR \quad (36)$$

by hydrogen atom transfer from an intermediate 17- or 19-electron dihydrogen adduct: $(H_2)Co(CO)_3$, $H_2Co(CO)_3$, or $(H_2)Co(CO)_4$. An odd-electron dihydrogen intermediate of this type is consistent with the promotional effect[44] of $^{\bullet}Co(CO)_4$ on the dehydrogenation of $HCo(CO)_4$. Furthermore, olefins are efficient hydrogen atom acceptors[35b,38] in the radical pair bond homolysis reactions of $HCo(CO)_4$ and $HMn(CO)_5$. However, these latter reactions generally are limited to activated olefins where the thermodynamics for the reaction in eq 37 is favorable.[9a,24a,45] For any

$$HCo(CO)_4 + CH_2{=}CHR \rightarrow {}^{\bullet}Co(CO)_4 + CH_3\dot{C}HR \quad (37)$$

given olefin, the proposed radical propagation reaction in eq 36 is thermodynamically more favorable by 14 kcal/mol than the established radical pair reaction in eq 37, based on the Co–H BDE in Table 2. Thus, the reaction in eq 36 should be applicable to a wider range of olefins, although there are no documented examples for the proposed[42] reaction type in eq 36.

Experimental Section

The high-pressure NMR probe and general sample handling procedures have been described previously.[3,4,13,15] The probe was modified for the magnetic susceptibility measurements by the addition of a small glass capillary. The capillary was 2.54 cm in length with a 5-mm o.d. This capillary was mounted vertically in the pressure vessel using a mounting socket that was machined from vespel (SP-1 polyimide). The capillary was held firmly in place within the mounting socket with a set screw, which was also machined from vespel. Similarly, the vespel mounting socket was securely fastened to the lid of the pressure between adjacent turns of a four-turn toroid detector with a bolt made of Be–Cu.

Line Shape Calculations. The theoretical NMR line shapes were calculated according to an analytical expression,[46] eq 3 of ref 46b, which was originally developed by Gutowsky *et al.* in a classical treatment that incorporated nuclear site exchange into the solutions of the Bloch equations. The same analytical function for the NMR line shape results for the special case of two uncoupled groups of magnetically equivalent nuclei from a quantum mechanical solution of the nuclear spin site exchange process in the density matrix formulation developed by Kaplan.[47] The theoretical line shape in eq 3 of ref 46b depends on seven input parameters: a vertical scale factor, the resonance frequencies for the two types of nuclei, the full line width at half-height in the absence of chemical exchange for both of the components, the fractional amount for component A, and the reduced exchange lifetime or τ. The reduced exchange lifetime is defined in terms of the lifetimes of the two components (τ_A, τ_B) and the mole fractions (f_A, f_B), according to the related expressions, $\tau = \tau_A\tau_B/(\tau_A + \tau_B)$, $\tau = f_A\tau_B$, and $\tau = f_B\tau_A$. Any of the seven spectral parameters which control the theoretical line shape may be varied in fitting the calculated curves to the observed spectra. The least-squares refinement[48] was based on the matrix formulation of Hamilton.[49] For the usual situation, only the vertical scale factor and the reduced exchange lifetime, τ, need to be refined in the least-squares fit because the other parameters are readily determined from the slow-exchange spectral data.

Cobalt Center Exchange. The theoretical NMR line shapes were calculated on the basis of opposing first-order rate processes for the two-site exchange equilibrium of eq 6 in the Results section. For example, the $H^{*}Co(CO)_4$ lifetime was analyzed on the basis of a first-order decay in the $H^{*}Co(CO)_4$ concentration. The mechanistic possibilities for effecting the net cobalt center exchange of eq 6 are presented in the Discussion section, where the justification for employing a first-order rate law for the process in eq 6 is given in the steady-state analysis of eqs 27 and 28. The calculations of the theoretical line shapes for the cobalt center exchange were performed using 2200 Hz for the full peak width at half-height in the absence of chemical exchange for the ^{59}Co NMR spectra. The chemical shifts were −2200 ppm for $Co_2(CO)_8$ and −3055 ppm for $HCo(CO)_4$. The fraction of $Co_2(CO)_8$ was refined as a variable in the least-squares fit, in addition to the vertical scale factor and the reduced exchange lifetime, τ. It was necessary to also refine the fractional composition because the ratio of $Co_2(CO)_8$ to $HCo(CO)_4$ changes with temperature.[13] Note that the actual exchange lifetime for the cobalt center in the $Co_2(CO)_8$ complex is obtained from the observed exchange lifetime, τ_A, from the least-squares fit to the experimental data by dividing the latter with the statistical factor[50] of 2. The discussion in the main body of the text only deals with the lifetime of the cobalt center in the $HCo(CO)_4$ complex, which requires no statistical correction factor.

Hydride Ligand Exchange. The hydride ligand exchange reaction between $HMn(CO)_5$ and $HCo(CO)_4$ was investigated in supercritical carbon dioxide, as previously described.[15] The solutions of the hydrides were prepared by allowing 0.015 M of $Mn_2(CO)_{10}$ and 0.018 M of $Co_2(CO)_8$ to reach equilibrium under 1.4 M of H_2 and 1.4 M of CO (or 4.1 M of CO) in supercritical carbon dioxide at a fluid density of 0.5 g/mL. The ^1H NMR spectra were analyzed by line-shape analysis. The full peak widths at half-height and the resonance frequencies that were used in the theoretical line-shape calculations are as follows: $HMn(CO)_5$, 51.78 Hz and −7.84 ppm; $HCo(CO)_4$, 45.97 Hz and −11.70 ppm. The hydride line widths are larger than that for the water or dihydrogen, presumably because the hydride resonances are broadened by scalar coupling to the quadrupolar metal nuclei.[17b] However, the temperature dependence of this latter effect is small for the complexes under study, as confirmed by investigating each metal system independently. Thus,

(42) If at least one of the reactions which produce $HCo(CO)_4$ as well as one of the reactions which consume this hydride is first-order in the olefin, then the steady-state $HCo(CO)_4$ concentration can be nearly constant over a large range of olefin concentrations, consistent with our observations.[4,5] In addition, Pino's isotope distribution results[7] employing D_2 and $HCo(CO)_4$ are also consistent with the presence of alkyl radicals in the hydroformylation system and warrants further investigation. Thus, the RCO radical, which proposedly is produced under D_2 and CO by carbonylation of the alkyl radical from the reaction in eq 36, will be labeled with deuterium. This labeled RCO radical is expected to extract a hydrogen atom from $HCo(CO)_4$, generating an aldehyde product which is preferentially labeled with hydrogen at the aldehyde moiety and deuterium in the alkyl chain, consistent with Pino's experimental observations; see Scheme 10 of ref 7 for more details. It is noted that hydrogen atom transfer from $HCo(CO)_4$ to an olefin-substituted tricarbonylcobalt radical has been suggested[43] as the rate-limiting step in the formation of tetracarbonylalkylcobalt compounds. Furthermore, the similarity of this latter mechanism to the proposed hydrogen atom transfer process in eq 36 suggests that the complete manifold of atom transfer reactions in the hydroformylation system possibly is quite extensive. However, both the steady-state $HCo(CO)_4$ concentrations and Pino's isotope results require an additional process, such as the hydrogen atom transfer reaction in eq 36. To our knowledge, there are no documented examples of the proposed hydrogen atom transfer reaction in eq 36.

(43) Ungváry, F.; Sisak, A.; Markó, L. In *Homogeneous Transition Metal Catalyzed Reactions*; Moser, W., Slocum, D., Eds.; *Advances in Chemistry 230*; American Chemical Society: Washington, DC, 1992; Chapter 20 and references therein.

(44) (a) Ungváry, F.; Markó, L. *J. Organomet. Chem.* **1980**, *193*, 383–387. (b) Wegman, R. W.; Brown, T. *J. Am. Chem. Soc.* **1980**, *102*, 2494–2495. (c) Clark, A. C.; Terapane, J. F.; Orchin, M. *J. Org. Chem.* **1974**, *39*, 2405.

(45) Bullock, R. M.; Samsel, E. G. *J. Am. Chem. Soc.* **1990**, *112*, 6886–6898.

(46) (a) Gutowsky, H. S.; McCall, D. W.; Slichter, C. P. *J. Chem. Phys.* **1953**, *22*, 279–292. (b) Gutowsky, H. S.; Holm, C. H. *J. Chem. Phys.* **1956**, *25*, 1228–1234.

(47) Kaplan, J. I.; Fraenkel, G. *NMR of Chemically Exchanging Systems*; Academic Press: New York, 1980; Chapter 6.

(48) A FORTRAN listing of the least-squares line-shape analysis subroutine is available upon request.

(49) Hamilton, W. C. *Statistics in Physical Science; Estimation, Hypothesis Testing, and Least Squares*; Ronald Press Co.: New York, 1964.

(50) Basolo, F.; Pearson, R. G. *Mechanisms of Inorganic Reactions. A Study of Metal Complexes in Solution*; John Wiley and Sons, Inc.: New York, 1968; Chapter 7.

the line width for the hydride resonance in $HCo(CO)_4$ is nearly invariant with temperature in the absence of $HMn(CO)_5$, as indicated at 180 °C in Figure 4. Similarly, the line width for the hydride resonance in $HMn(CO)_5$ does not vary significantly with temperature in the absence of $HCo(CO)_4$.

The ^{55}Mn longitudinal spin relaxation times (T_1) for $Mn_2(CO)_{10}$ and $HMn(CO)_5$, which were measured by the inversion–recovery pulse sequence,[17b] at 100 °C and 257 atm pressure are 76 and 1.08 ms, respectively. Therefore, the alternative NMR magnetization transfer technique was not used in an attempt to lower the upper limit for the rate of manganese center exchange in this system because $T_1 \approx T_2$. Thus, a chemical exchange process cannot be measured by an NMR line-width analysis[17] if the chemical lifetime is much longer than the transverse spin relaxation time, $\tau > T_2$. Similarly, it is not possible to measure the chemical exchange process by the alternative NMR technique, magnetization transfer,[21] if the chemical exchange lifetime is much longer than the longitudinal spin relaxation time, $\tau > T_1$.

Carbonyl Ligand Exchange. The carbonyl exchange reaction has been followed qualitatively in supercritical carbon dioxide[3,13] and in pure carbon monoxide[5] solvents. The resonances for the free and coordinated carbon monoxide were observed to merge at approximately 140 °C. In these single-phase systems, the concentration of the free carbon monoxide is quite large in comparison to the coordinated carbon monoxide. Therefore, it is difficult to perform a line-shape analysis. Furthermore, the concentration of the free carbon monoxide cannot be lowered because carbon monoxide pressures in excess of 180 atm must be maintained to avoid irreversible decomposition of the $Co_2(CO)_8$ at 190 °C. Therefore, the carbonyl exchange reaction was investigated in mesitylene solvent. This two-phase system increases the concentration of the coordinated carbonyl groups relative to the free carbon monoxide in the solution phase so that the two resonances have approximately equal areas in the ^{13}C NMR spectra.

A solution of $Co_4(CO)_{12}$ (0.0583 M) in 6.0 mL of mesitylene solvent was loaded into the NMR pressure vessel in an inert-atmosphere glovebox. Subsequently, the $Co_4(CO)_{12}$ was converted to $Co_2(CO)_8$ by reaction with an excess of carbon monoxide at 100 °C. The final carbon monoxide pressure after complete conversion was 201.6 atm at 25 °C. This method of sample preparation was chosen to maximize the purity of the resultant $Co_2(CO)_8$ solution. Thus, $Co_4(CO)_{12}$ is easer to work with because it is more stable at ambient pressure than $Co_2(CO)_8$. Furthermore, $Co_4(CO)_{12}$ is readily converted to $Co_2(CO)_8$ in the high-pressure NMR probe.

The ^{13}C NMR resonances for the coordinated carbonyl ligand in $Co_2(CO)_8$ exhibits a small temperature-dependent chemical shift due to changes in the relative equilibrium concentrations[22] for the bridging and terminal carbonyl group. The ^{13}C chemical shifts were measured relative to the unique aromatic carbon in the mesitylene solvent that carries the methyl group at 137.4 ppm. The chemical shift for the coordinated carbonyl group is described by the relationship $\nu(Hz) = 15034.6 + 41590/T$ in the temperature range 298–353 K, where there is no significant line broadening due to carbonyl exchange with free carbon monoxide. This empirical relationship was extrapolated to obtain the chemical shift for the coordinated carbonyl groups in the 100–190 °C range. Furthermore, this correction for the temperature dependence of the chemical shift for the carbonyl ligands had very little effect on the resultant rate constants for carbon monoxide exchange from the least-squares analysis in Figure 13, because none of the resultant rate constants changed by more than 10% when the calculations were repeated using a constant value of 15 173.7 Hz for the chemical shift of the coordinated carbonyl ligand. The natural line widths which were used in calculating the theoretical curves in Figure 13 were 35.39 and 15.07 Hz for the coordinated and free carbon monoxide, respectively. The line width of the coordinated carbonyl ligand is larger than that for the free carbon monoxide due to scalar coupling to the cobalt nucleus.[51] Furthermore, this broadening due to scalar coupling may vary with temperature.[17b] However, the resultant uncertainty in the natural line width for the coordinated carbonyl ligand appears to have a minimal effect on the calculated carbonyl exchange rate constants. This is because the values obtained by fitting only the resonance for the free carbon monoxide (which will not be broadened by scalar coupling) over the spectral range 193 to 178 ppm agree to within 5% over the entire temperature range 100–180 °C with the rate constants obtained by fitting the complete spectral window containing both free and coordinated carbon monoxide from 211 to 175 ppm. Similarly, Roe[11] has previously noted that the carbonyl exchange

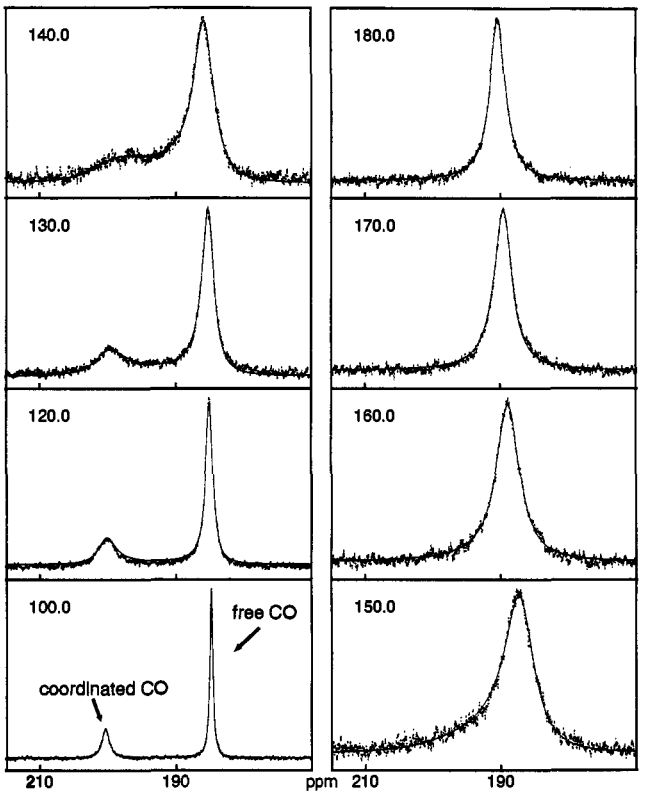

Figure 13. Calculated and observed ^{13}CO NMR spectra for carbonyl exchange in $Co_2(CO)_8$.

rate constant can be determined by fitting only the line width of the free carbon monoxide. Similarly, Lichtenberger and Brown[51] have obtained chemical exchange rate data in the presence of scalar coupling within the ^{13}C NMR spectra for compounds of the form $(CO)_4CoEX_3$ (where E = C, Si, Ge, Sn, or Pb and X = F, Cl, CH_3, C_4H_9, $CH_2C_6H_5$, or C_6H_5). In addition, as noted in the Discussion section, the rate constants which are compiled in Table 7 of the supplementary material are consistent with the values obtained by other methods. Thus, the rate constants in Table 7 may be fit along with those obtained by ^{14}CO tracer studies,[10] by ^{13}CO NMR magnetization transfer,[11] and by $AsPh_3$ substitution[26a] with a single line (correlation coefficient 0.996) in an Arrhenius plot that covers a range of −20 to 180 °C.

Magnetic Susceptibility Measurements. The solution of $Co_2(CO)_8$ which was used for the magnetic susceptibility measurement was prepared from $Co_4(CO)_{12}$, as described above. Furthermore, the measurement of the $Co_2(CO)_8$ magnetic susceptibility required a slight modification of the Evan's method. Methane was used as the reference peak for the $Co_2(CO)_8$ determination. However, the glass capillary was filled to 0.082 M with only the reference material, methane. This contrasts with the standard Evan's methodology,[12] where both compartments of the standard coaxial NMR tube contain the complete solvent mixture. In the $Co_2(CO)_8$ experiment, the main compartment of the NMR pressure probe was filled with methane, 0.30 M; carbon monoxide, 9.95 M; and $Co_2(CO)_8$, 0.0443 M. Therefore, the pressure within the capillary was much lower than that in the main compartment of the NMR probe. Consequently, there was a substantial difference in the volumetric susceptibilities of the media in the two compartments, even in the absence of radical formation. However, the frequency difference between the methane resonances in the capillary and the bulk sample in any given ^1H NMR spectrum is still proportional to the difference in the volumetric susceptibilities of the media in the two compartments according[52] to eq 38 The geometric factor of $4\pi/3$ in eq 38, which is appropriate for a

$$\frac{\Delta\nu}{\nu_0} = \frac{4\pi}{3}(\chi_v - \chi_v(\text{cap})) \qquad (38)$$

parallel applied magnetic field[12b] and is sometimes treated as an adjustable parameter, was confirmed to be accurate for the high-pressure probe geometry using standard solutions of $Cr(Acac)_3$. Furthermore, on the

(51) Lichtenberger, D. L.; Brown, T. L. *J. Am. Chem. Soc.* **1977**, *99*, 8187–8194.

(52) Dickinson, W. C. *Phys. Rev.* **1951**, *81*, 717.

basis of the sensitivity of the frequency shifts for $Cr(AcAc)_3$, we estimate that radicals with a single unpaired electron can be measured at concentration levels of approximately 10^{-3} M with the toroid NMR detector. Furthermore, the frequency difference based on the resonances for the gaseous methane reference is a sufficiently sensitive experimental probe to enable the measurement of the molar susceptibility of a gaseous diamagnetic substrate. Thus, the frequency difference, $\Delta\nu$, between the two methane resonances responded linearly at 24 °C to incremental changes, $\Delta p = 33.8$ atm, in the carbon monoxide pressure probe ranging from 50.3 Hz at 67.4 atm to 134.7 Hz at 236.6 atm. These frequency differences yield, with the aid of eq 38 and an appropriate units conversion, a measured molar susceptibility for carbon monoxide of $(-0.36 \pm 0.01) \times 10^{-6}$ cgs units in agreement with the literature value[53] of -0.35×10^{-6} cgs units.

As the temperature is increased above 25 °C for the carbon monoxide solution which contains the solid $Co_2(CO)_8$ sample, the frequency separation ($\Delta\nu$) between the two methane resonances initially begins to increase as the $Co_2(CO)_8$ progressively dissolves in the carbon monoxide solvent. This diamagnetic shift results due to an increase in the volumetric susceptibility of the gas-phase solution with the dissolution of the $Co_2(CO)_8$. In the complete absence of radical formation, this diamagnetic shift is estimated to be 6.1 Hz on the basis of a molar susceptibility for $Co_2(CO)_8$ of 110×10^{-6} cgs units which was obtained from Pascal's constants.[54] The dissolution of the $Co_2(CO)_8$ is complete by 120 °C, and $\Delta\nu$ begins to decrease consistent with the production of a paramagnetic species. For comparison, the solubility of $Co_2(CO)_8$ in carbon monoxide was independently measured[55] by the method previously described for supercritical carbon dioxide.[13] The shifts that are compiled in column 2 of Table 8 in the supplementary material are relative to the methane frequency separation, $\Delta\nu$, at 25 °C. By 180 °C, the paramagnetic shift due to radical formation is approximately equal in magnitude to the diamagnetic shift due to the dissolution of the $Co_2(CO)_8$ complex, leading to a net methane frequency separation, $\Delta\nu$, which is nearly the same as that observed at 25 °C. The frequency shifts in column 2 of Table 8 were used with eq 38 to calculate the volumetric susceptibility. The resultant χ_v was converted to the susceptibility per equivalent of $Co(CO)_4$ and corrected for diamagnetism in column 3 of Table 8, based[54] on -9.8×10^{-6} cgs units per carbonyl and -16×10^{-6} cgs units for the cobalt. The $^{\bullet}Co(CO)_4$ radical concentrations in column 4 were calculated according to eq 39, where the molar susceptibility for the $^{\bullet}Co(CO)_4$ radical, χ_M,

$$[^{\bullet}Co(CO)_4] = \frac{[\text{total cobalt}]\chi_{corr}}{\chi_M} \tag{39}$$

is calculated[12c] with Curie's law using the spin-only magnetic moment of 1.73 μ_B. The $Co_2(CO)_8$ concentration was calculated by subtracting half of the $^{\bullet}Co(CO)_4$ radical concentration from the initial cobalt loading. The values in Table 8 indicate that the $Co_2(CO)_8$ complex is approximately 5% dissociated at 175 °C.

Effect of $^{\bullet}Mn(CO)_5$ Radical Intermediate on the ^{55}Mn NMR Line Widths. For the case of an intermediate with an unpaired spin, such as the $^{\bullet}Mn(CO)_5$ radical of eqs 19 and 20 of Scheme 3, the necessary criterion[56] for slow exchange on the NMR time scale is given by the inequality in eq 40, where $\tau_{Mn\cdot}$ is the lifetime of the $^{\bullet}Mn(CO)_5$ radical

$$\left(\frac{\delta\omega\tau_{Mn\cdot}}{2}\right)^2 \gg 1 \tag{40}$$

and $\hbar\delta\omega$ is the energy of the magnetic hyperfine interaction between the unpaired electron spin and the manganese nucleus in $^{\bullet}Mn(CO)_5$. If the inequality in eq 40 is not established, then the line width will be given[57] by eq 41 instead of the slow exchange approximation in eq 8. Furthermore,

$$W_{1/2}(\text{obs}) = W_{1/2}^{*} + \frac{(\delta\omega\tau_{Mn\cdot})^2}{\pi\tau_{HMn(CO)_5}} \tag{41}$$

if the reactions in eqs 19 and 20 are effectively at steady state, then the lifetime of the $^{\bullet}Mn(CO)_5$ radical is given by eq 42. Therefore, according

$$\tau_{Mn\cdot} = \frac{[^{\bullet}Mn(CO)_5]\tau_{HMn(CO)_5}}{[HMn(CO)_5]} \tag{42}$$

to eqs 41 and 42 the chemical exchange broadening of the $HMn(CO)_5$ resonance in the ^{55}Mn NMR spectra will decrease as the square of the radical concentration if the inequality in eq 40 is not established. The relevant parameters $\delta\omega$ and $\tau_{Mn\cdot}$ are not known, but reasonable estimates may be made for them. The concentration of the $^{\bullet}Mn(CO)_5$ radical is estimated to be 10^{-9} M on the basis[27] of a 38 ± 5 kcal/mol Mn–Mn BDE in $Mn_2(CO)_{10}$. The lifetime of the $HMn(CO)_5$ complex is already only 10^{-3} to 10^{-4} s, according to Figure 6. Thus, $\tau_{Mn\cdot}$ is estimated to be 10^{-10} to 10^{-11} s^{-1}, on the basis of eq 42. The hyperfine coupling constant $\delta\omega$ is estimated to be 1×10^9 rad s^{-1} on the basis of the other manganese radicals.[58] Thus, the product of the estimated values for $\delta\omega$ and $\tau_{Mn\cdot}$ would be too small to establish the inequality of eq 40. Furthermore, the lack of significant broadening for the $HMn(CO)_5$ resonance in the ^{55}Mn spectra suggests that the inequality of eq 40 is not established in the temperature range covered in this investigation due to the low $^{\bullet}Mn(CO)_5$ radical concentration.

Acknowledgment. We thank Professors J. Halpern, C. Hoff, M. Baird, T. Brown, and F. Ungváry and Dr. M. Bullock for helpful discussions and correspondence. In addition, we thank one of the reviewers for suggesting a variant of the oxidative addition reaction mechanism that is used as an example in the manuscript. Support for this work was provided by the Office of Basic Energy Sciences, Division of Chemical Sciences, U.S. Department of Energy, under Contract W-31-109-ENG-38.

Supplementary Material Available: Tables 5–8, listing kinetic, line width, and magnetic susceptibility data (4 pages). This material is contained in many libraries on microfiche, immediately follows this article in the microfilm version of the journal and can be ordered from the ACS; see any current masthead page for ordering information.

(53) *Handbook of Chemistry and Physics*, 49th ed.; Chemical Rubber Co.: Cleveland, OH, 1968; p E-129.

(54) Selwood, P. W. *Magnetochemistry*; Interscience Publishers Inc.: New York, 1956.

(55) The resultant solubility parameters, $\Delta H = 7.2$ kcal/mol and $\Delta S = 12$ eu, indicate that the $Co_2(CO)_8$ should be dissolved by 120 °C, even though the carbon monoxide concentration, 7.12 M, used for the solubility determination was lower than that which was used for the magnetic susceptibility measurement, 9.95 M.

(56) (a) McConnell, H. M.; Weaver, H. E. *J. Chem. Phys.* **1956**, *25*, 307. (b) McConnel, H. M.; Berger, S. B. *J. Chem. Phys.* **1957**, *27*, 230–234.

(57) Kreilick, R. W.; Weissman, S. I. *J. Am. Chem. Soc.* **1962**, *84*, 306–307.

(58) (a) Anderson, O. P.; Symons, M. C. R. *J. Chem. Soc., Chem. Commun.* **1972**, 1020. (b) Fieldhouse, S. A.; Fullam, B. W.; Neilson, G. W.; Symons, M. C. R. *J. Chem. Soc., Dalton Trans* **1974**, 567–569. (c) Kochi, J. K. *Organometallic Mechanism and Catalysis*; Academic Press: New York, 1978; Chapter 3.